이학박사학위논문

인간 거대세포바이러스 감염 시 noncoding RNA의 기능

Role of Intergenic Noncoding RNA During Human Cytomegalovirus Infection

2015년 2월

서울대학교 대학원

생명과학부

이 상 현

CONTENTS

CONTENTS I

LIST OF TABLES AND FIGURES III

LIST OF ABBREVIATIONS VI

I. ABSTRACT 1

II. INTRODUCTION 3

1. Human Cytomegalovirus 3
2. microRNA (miRNA) 7
3. Polycistronic feature of miRNAs 10
4. Systemic approach to study the interplay between cellular miRNAs and HCMV clinical strain 11

III. RESULTS 14

1. The HCMV clinical strain differentially regulates the expression of the miR-17-92 cluster 14
2. HCMV infection induced primary transcription of the miR-17-92 cluster, followed by the selective downregulation of mature miR-17 and miR-20a 28

CONTENTS (*CONTINUED*)

3. HCMV clinical strain-specific RNA mediates the turnover of the miR-17 and miR-20a through sequence-specific RNA-miRNA interactions 38

4. Identification of a miRDE that directs the turnover of miRNA through non-canonical miRNA-mRNA interactions 52

5. miR-17 binding-site mutant HCMV loses the ability to differentially regulate the miR-17-92 cluster 64

6. miRDE-mediated regulation of the miR-17 family results accelerates virus production 72

IV. DISCUSSION 84

V. EXPERIMENTAL PROCEDURES 90

VI. REFERENCES 105

VII. ABSTRACT IN KOREAN 110

VIII. APPENDIX 112

LIST OF FIGURES

Figure 1.	HCMV genome and viral miRNAs	5
Figure 2.	Model of miRNA biogenesis and functions	8
Figure 3.	Schematic feature of miRNA microarray during HCMV infection	13
Figure 4.	Changes in miRNA expression upon HCMV infection	16
Figure 5.	Expression of the primary and mature forms of miRNAs modulated by HCMV	18
Figure 6.	Organization of the miR-17-92 cluster	20
Figure 7.	Individual miRNA levels in miR-17-92 cluster during Toledo infection	22
Figure 8.	Expression of miR-17 family during Toledo-WT/Δ15kb infection	24
Figure 9.	miR-17-92 cluster expression during AD169 infection	26
Figure 10.	Primary miR-17-92 levels during Toledo infection	30
Figure 11.	Functions of IE1/2 within miR-17-92 induction	32
Figure 12.	Expression of the precursor and mature form of	34

miR-17 and miR-20a during Toledo infection

Figure 13. miR-17* and miR-20a* expression during Toledo infection 36

Figure 14. Drug-sensitivity assay 42

Figure 15. Clone recovery test with ToledoΔ15kb 44

Figure 16. Identification of UL144-145 transcript as a decay factor of miR-17 family 46

Figure 17. Retargeting UL144-145 to other miRNAs in miR-17-92 cluster 48

Figure 18. Predicted 3D RNA structure of UL144-145 intergenic region 50

Figure 19. Intergenic region is sufficient to degrade miR-17 and miR-20a 54

Figure 20. Non-canonical interaction between miR-17 family and UL144-145 intergenic region 56

Figure 21. Deletion screening to identify the minimal requirement for miR-17 decay 58

Figure 22. 50 nt RNA oligomers is sufficient to function as miR-17 decay element 60

Figure 23. miRDE (miRNA Decay Element) in HCMV 62

genome

Figure 24. A Mutant virus with triple base substitution in the miR-17 binding site 66

Figure 25. miRNA stability assay with WT or mutant virus infection 68

Figure 26. Knock-down effect of a specific Ago on the miRDE-mediated miR-17 decay 70

Figure 27. Degradation of miR-17 by miRDE is essential for the rapid viral production during lytic infection 74

Figure 28. Apoptosis rate during Toledo-WT and ToledoΔ17Seed infection 76

Figure 29. Rescue experiment using an anti-sense oligomer against miR-17 and miR-20a during Toledo infection 78

Figure 30. Sequence comparison of miRDE in the UL144-145 intergenic region of HCMV clinical isolates 80

Figure 31. Schematic summary 82

Table 1. Primer information 97

LIST OF ABBREVIATIONS

HCMV	Human Cytomegalovirus
miRNA	microRNA
miRDE	miRNA Decay Element
Toledo	A clinical strain of HCMV
ORF	Open reading frame
Pri-miRNA	Primary miRNA
Pre-miRNA	Precursor miRNA
HFF	Human foreskin fibroblast
MOI	Multiplicity of infection
qRT-PCR	quantitative RT-PCR
hpi	hours post-infection
IE1	HCMV Immediate early protein 1
IE2	HCMV Immediate early protein 2
Act D	Actinomycin D
CHX	Cycloheximide
ToledoΔ17seed	The miR-17 binding site mutant virus of Toledo
gB	HCMV glycoprotein B

I. ABSTRACT

Sanghyun Lee

School of Biological science
The Graduate school
Seoul National University

Virulence of human cytomegalovirus (HCMV) clinical isolates correlates with carriage of a 15-kb segment in the UL/b' region of the viral genome, which is absent from attenuated strains. The mechanisms by which this segment contributes to HCMV virulence remain obscure. I observed that intergenic RNA sequences within the 15-kb segment function as a microRNA (miR) decay element (miRDE) and direct the selective, sequence specific, turnover of mature miR-17 and miR-20a encoded within the host miR-17-92 cluster. Unlike canonical miRNA-mRNA interactions, the miRNA-miRDE interactions did not repress miRDE expression. miRNA binding site mutations retargeted miRDE to other miR-17-92 cluster miRNAs, which are otherwise resistant to miRDE-mediated decay. miRDE function was required to accelerate virus production in the context of lytic HCMV infection. These results indicate a role for viral noncoding RNA in regulating cellular miRNAs during

HCMV pathogenesis, and suggest that noncoding RNAs may play a role in mature miRNA turnover.

Keywords: *HCMV, miRNA, miR-17-92, miRDE, Decay, and viral production.*

Student Number: *2008-22751*

II. INTRODUCTION

1. Human Cytomegalovirus

Human cytomegalovirus (HCMV) is a member of the β-herpesvirus subfamily and a ubiquitous human pathogen. After primary infection, HCMV establishes a lifelong latent infection in bone marrow-derived CD34 (+) progenitors and peripheral blood to CD14 (+) monocyte (Sinclair and Sissons, 2006). HCMV infections in healthy individuals are typically asymptomatic and remain the leading cause of birth defects and the major cause of infectious mortality and morbidity in immune-compromised patients (Britt, 2008). Historically, HCMV research has primarily relied on attenuated strains (AD169 and Towne) extensively passaged in fibroblasts (Goodrum et al., 2007). Attenuated HCMV strains have acquired genome rearrangements that distinguish them from HCMV clinical strains. For example, the genome of the HCMV clinical strain Toledo contains an additional 15-kb segment in the UL/b' region, which is present in all virulent strains but not in the attenuated strain AD169 (Murphy et al., 2003). HCMV clinical strains and attenuated strains have striking differences in virulence and cell tropism. The 15-kb segment

plays a critical role in clinical pathogenesis *in vivo* and contains at least 19 open reading frames (ORFs) and 1 viral microRNA (miRNA). The functions of the viral genes encoded in the 15-kb segment are associated with cell tropism (Hahn et al., 2004; Revello and Gerna, 2010), latency (Goodrum et al., 2007), cytokine regulation (Kim et al., 2012; Penfold et al., 1999), and NK cell responses (Wills et al., 2005). However, the mechanisms underlying the high virulence of the clinical strains remain poorly understood (Figure 1). HCMV

Figure 1. HCMV genome and viral miRNAs

(A) The schematic view of HCMV genomes. Attenuated strains, such as AD169 and Towne, lost ~15 kb genomic segment. The ~15 kb contains at least 19 ORFs (UL136 ~ UL150) and 1 viral miRNA (miR-UL148D). The attenuated strains have lost the clinical infectivity.

(B) HCMV viral miRNAs, predicted and reported, are shown on HCMV genome map. 11 miRNA hairpins are transcribed during HCMV lytic infection. All of those miRNAs show early gene expression kinetics.

A

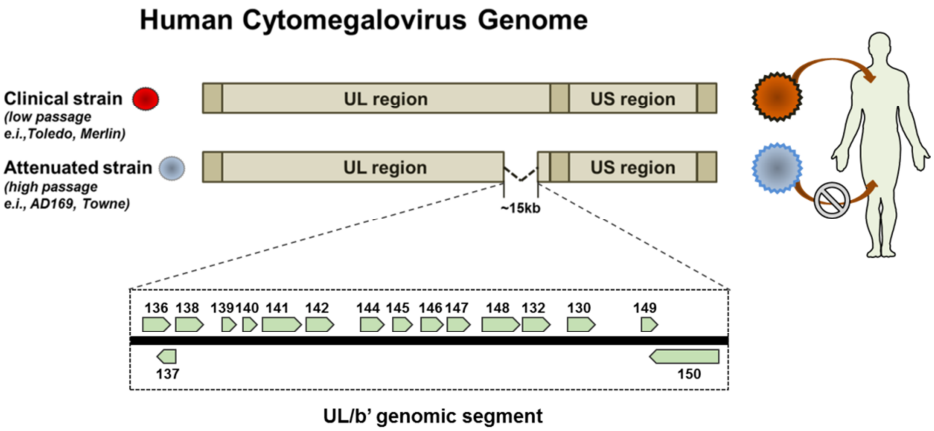
Human Cytomegalovirus Genome
Clinical strain
(low passage
e.i.,Toledo, Merlin)
UL region
US region
Attenuated strain
(high passage
e.i., AD169, Towne)
UL region
US region
~15kb
136 138 139 140 141 142 144 145 146 147 148 132 130 149
137
150
UL/b' genomic segment

B

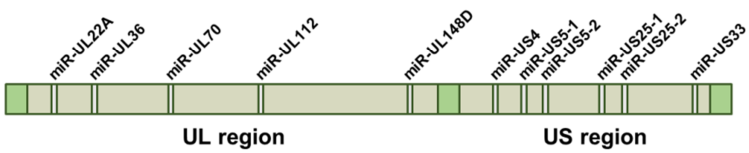
miR-UL22A
miR-UL36
miR-UL70
miR-UL112
miR-UL148D
miR-US4
miR-US5-1
miR-US5-2
miR-US25-1
miR-US25-2
miR-US33
UL region
US region

2. MicroRNA (miRNA)

miRNA is an approximately 22-nucleotide (nt) noncoding RNA that regulates gene expression at the post-transcriptional level. The human genome is predicted to encode >1,000 miRNAs that regulate more than one-third of all human transcripts (Chang and Mendell, 2007). miRNAs are transcribed as long primary transcripts (pri-miRNAs) by RNA polymerase II (Lee et al., 2004) and cropped into hairpin-shaped RNA precursors (pre-miRNAs) by the nuclear RNase III Drosha (Lee et al., 2003). RNase III Dicer further processes pre-miRNAs in the cytoplasm into approximately 22-nt miRNA duplexes (Bernstein et al., 2001; Hutvagner et al., 2001; Ketting et al., 2001; Knight and Bass, 2001), one strand of which is typically incorporated into Argonaute proteins (Khvorova et al., 2003; Schwarz et al., 2003) (Figure 2). miRNA expression is primarily regulated at the transcriptional level and, in some cases, miRNA biogenesis might be regulated at the post-transcriptional level (Krol et al., 2010). The steady-state levels of miRNA are a function of biogenesis and turnover. In contrast to miRNA biogenesis, much less is known about the turnover of miRNAs.

Figure 2. Model of miRNA biogenesis and functions

Monocistronic and polycistronic miRNAs are processed by the followed pathway. Drosha, Exportin 5, and Dicer process the immature miRNAs from the nucleus to the cytosol. Typically, miRNAs are loaded into RISC, and then repress and cleavage the target mRNAs.

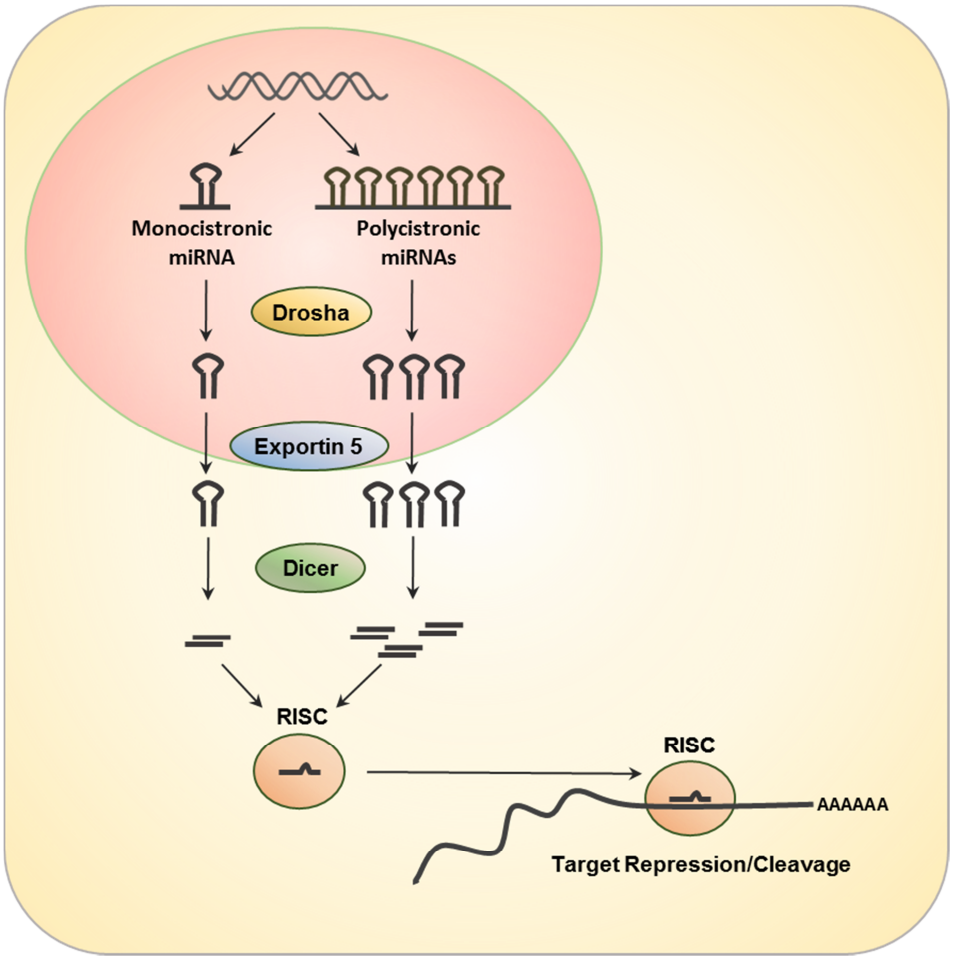
Monocistronic
miRNA
Polycistronic
miRNAs
Drosha
Exportin 5
Dicer
RISC
RISC
AAAAAA
Target Repression/Cleavage

3. Polycistronic feature of miRNAs

A prominent characteristic of miRNAs is that their genes are often closely clustered within the genome. More than 30% of human miRNAs are predicted to be encoded within polycistronic miRNA clusters (Altuvia et al., 2005). These clustered miRNAs are transcribed and processed from polycistronic primary transcripts (Figure 2). Most studies on clustered miRNAs have demonstrated their functional redundancy and coordinated regulation (Mendell, 2008). For example, the well-known miRNA cluster miR-17-92 encodes 6 miRNAs (miR-17, miR-18a, miR-19a, miR-20a. miR-19b-1, and miR-92a-1) that function as oncogenes (He et al., 2005). The expression of these miRNAs regulates the same cellular process to achieve homeostasis either individually or in a coordinated manner (Olive et al., 2010). The functional dissection of each miRNA has been performed using an *in vivo* tumorigenic model (Mavrakis et al., 2010; Mu et al., 2009; Olive et al., 2009; Shan et al., 2009). The key oncogenic component of the miR-17-92 cluster miR-19 induces lymphomagenesis by targeting the apoptotic genes Pten and Bim (Mavrakis et al., 2010; Mu et al., 2009; Olive et al., 2009). Furthermore, the overexpression of miR-17 results in reduced cell adhesion, migration, and proliferation (Shan et al., 2009). However, whether individual

miRNAs in a cluster undergo differential regulation at the post-transcriptional level and have distinct functions is not yet known.

4. Systemic approach to study the interplay between cellular miRNAs and HCMV clinical strain

To elucidate the pathogenesis of HCMV clinical strains, using miRNA microarray, I investigated virus-host miRNA interactions (Figure 3) and identified the cellular miRNA expression profile is converted during HCMV infection. I focused on the miRNA cluster, miR-17-92, which carries six miRNAs. HCMV selectively degrades the miR-17 family members of the miR-17-92 cluster and it accelerates virus production. These results show that the interplay between the viral noncoding RNA and cellular miRNAs might be important for elucidating HCMV pathogenesis.

Figure 3. Schematic feature of miRNA microarray during HCMV infection

miRNA microarray for cellular miRNA expression. miRNA microarray chip is produced by *Agilent biotech*. The microarray DNA chip was designed for detecting 887 cellular miRNAs and 17 HCMV miRNAs. HFF cells were infected with Toledo-WT or ToledoΔ15kb virus at 5 MOI. At 24 and 72 hpi, total RNAs were prepared for analysis.

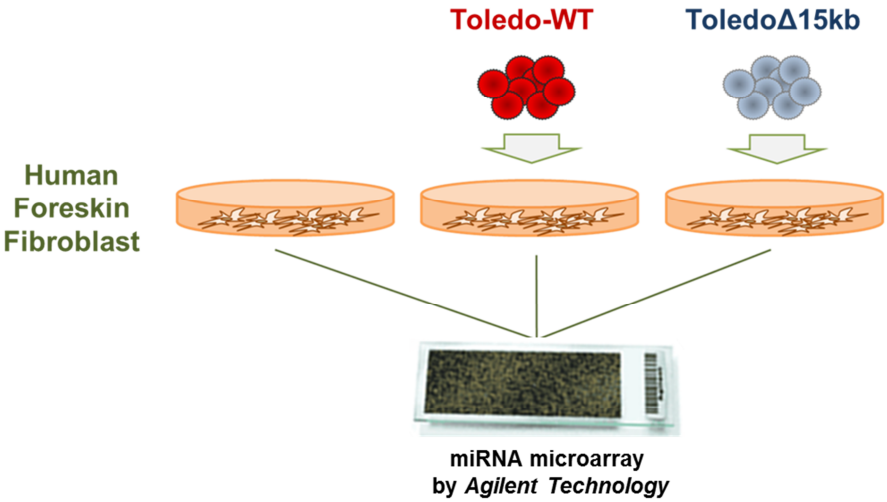
Toledo-WT
ToledoΔ15kb
Human
Foreskin
Fibroblast
miRNA microarray
by Agilent Technology

IV. RESULTS

1. The HCMV clinical strain differentially regulates the expression of the miR-17-92 cluster

miRNA microarrays were used to investigate host miRNA expression profiles during HCMV clinical strain infection. Human foreskin fibroblasts (HFFs) were infected with the HCMV clinical strain Toledo. To mimic the attenuated strain, I used ToledoΔ15kb, which lacks the 15-kb genomic segment in the UL/b' region (Wang et al., 2005). The miRNA expression profile showed that several host miRNAs were regulated during HCMV infection (Figure 4). miR-100, miR-199a-3p, miR-199a-5p, and miR-199b-5p were downregulated during infection with Toledo-wild type (WT) and ToledoΔ15kb, consistent with previously reported data (Santhakumar et al., 2010; Wang et al., 2008). Notably, I identified host miRNAs that were regulated during HCMV infection. miR-29a/b/c, miR-125b, miR-199a-3p, and miR-199a-5p were downregulated at the primary miRNA level (Figure 5).

Interestingly, I observed that Toledo-WT differentially regulated the

levels of mature miRNAs within the miR-17-92 cluster. The miR-17-92 cluster contains 6 miRNAs: miR-17, miR-18a, miR-19a, miR-20a, miR-19b, and miR-92a. These miRNAs are categorized into 4 miRNA families according to their seed sequences: miR-17 (miR-17 and miR-20a), miR-18 (miR-18a), miR-19 (miR-19a and miR-19b), and miR-92 (miR-92a) (Figure 6). Northern blotting and qRT-PCR analyses confirmed that Toledo-WT downregulated 2 homologous mature miRNAs, miR-17 and miR-20a, but upregulated miR-18a, miR-19a, miR-19b, and miR-92a (Figures 7A and B). The differential regulation of the miR-17-92 cluster occurred in Toledo-WT but not in ToledoΔ15kb-infected cells. ToledoΔ15kb infection increased the expression of the miR-17 and miR-20a (Figure 8). The attenuated HCMV strain AD169 exhibited results similar to those of ToledoΔ15kb. AD169 induced all six miRNAs in the miR-17-92 cluster during infection (Figure 9). These results demonstrate that the HCMV clinical strain Toledo differentially regulates the expression of miRNAs within the miR-17-92 cluster at the post-transcription level, indicating that the 15-kb region is responsible for the observed phenotype.

Figure 4. Changes in miRNA expression upon HCMV infection

Human foreskin fibroblasts (HFFs) were infected with Toledo-WT or ToledoΔ15kb for miRNA microarray (5 MOI). The miRNA expression levels of virus-infected HFFs at 24 or 72 hpi were compared with those for the noninfected control. The color scale is based on log2 changes in expression.

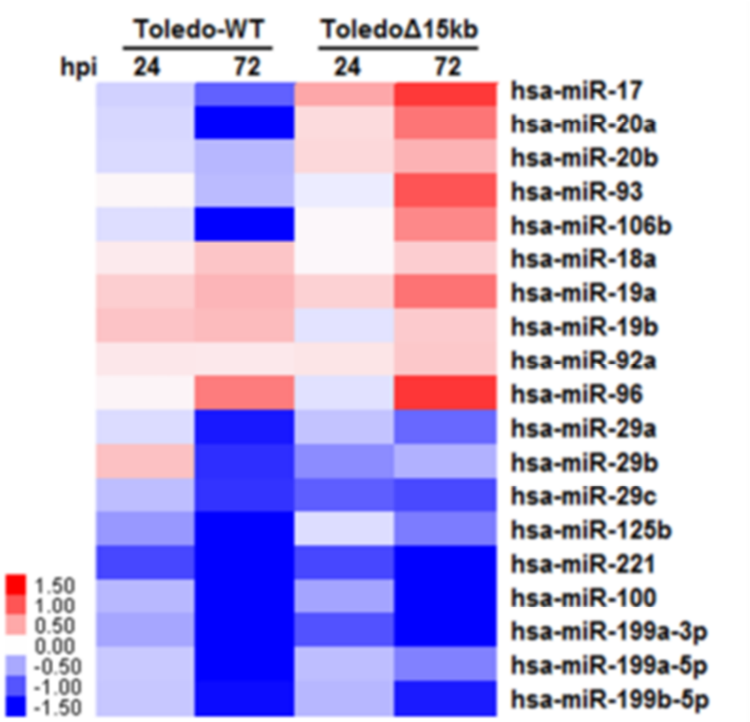
Toledo-WT
ToledoΔ15kb
hpi
24
72
24
72
hsa-miR-17
hsa-miR-20a
hsa-miR-20b
hsa-miR-93
hsa-miR-106b
hsa-miR-18a
hsa-miR-19a
hsa-miR-19b
hsa-miR-92a
hsa-miR-96
hsa-miR-29a
hsa-miR-29b
hsa-miR-29c
hsa-miR-125b
hsa-miR-221
hsa-miR-100
hsa-miR-199a-3p
hsa-miR-199a-5p
hsa-miR-199b-5p
1.50
1.00
0.50
0.00
-0.50
-1.00
-1.50

Figure 5. Levels of the primary and mature cellular miRNAs modulated by HCMV

(A) The expression levels of the cellular miRNAs during HCMV infection were detected using Northern blotting. Compared with the noninfected control, the miRNA expression levels of virus-infected HFFs at 24 or 72 hr post-infection (hpi) were downregulated. (B) The pri-miRNA levels of each miRNA were determined through qRT-PCR using specific primers for detecting primary miRNA transcripts.

A

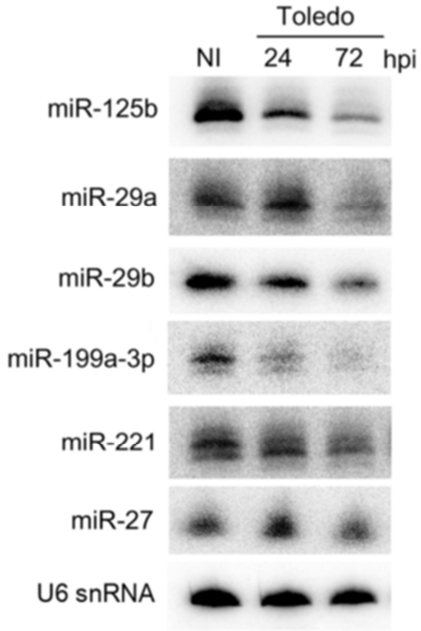
Toledo
NI
24
72
hpi
miR-125b
miR-29a
miR-29b
miR-199a-3p
miR-221
miR-27
U6 snRNA

B

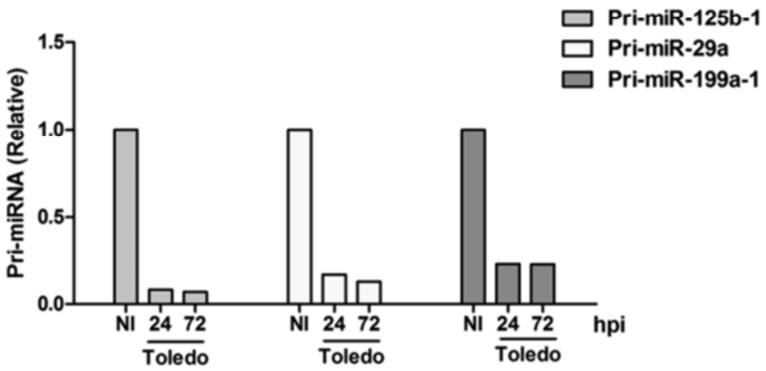
Pri-miR-125b-1
Pri-miR-29a
Pri-miR-199a-1
Pri-miRNA (Relative)
1.5
1.0
0.5
0.0
NI 24 72
Toledo
NI 24 72
Toledo
NI 24 72
Toledo
hpi

Figure 6. Organization of the miR-17-92 cluster

Organization of the miR-17-92 cluster. This cluster can be grouped into four families: miR-17 (miR-17 and miR-20a), miR-18 (miR-18a), miR-19 (miR-19a, b), and miR-92 (miR-92a). The seed sequences of miRNAs are indicated in bold. The primary miR-17-92 is encoded in the 3rd intron of C13orf25 gene.

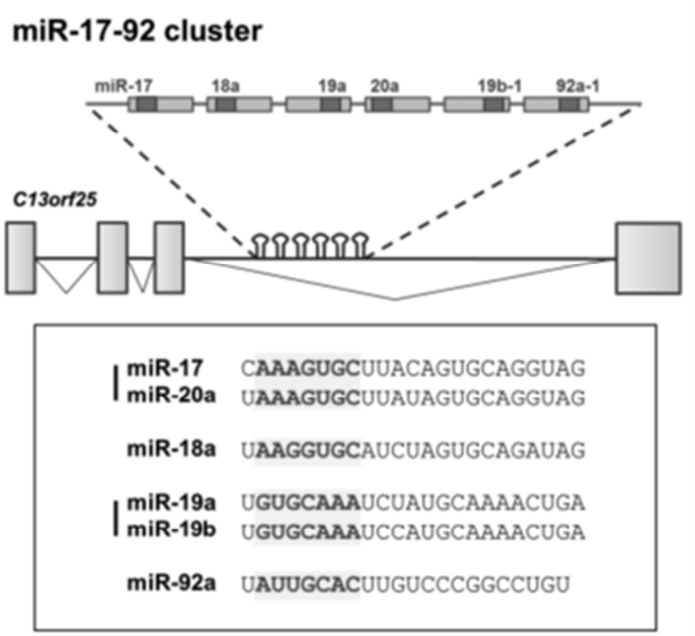
miR-17-92 cluster
miR-17
18a
19a
20a
19b-1
92a-1
C13orf25
miR-17 CAAAGUGCUUACAGUGCAGGUAG
miR-20a UAAAGUGCUUAUAGUGCAGGUAG
miR-18a UAAGGUGCAUCUAGUGCAGAUAG
miR-19a UGUGCAAAUCUAUGCAAAACUGA
miR-19b UGUGCAAAUCCAUGCAAAACUGA
miR-92a UAUUGCACUUGUCCCGGCCUGU

Figure 7. Individual miRNA levels in miR-17-92 cluster during Toledo infection

Northern blotting (A) and quantitative RT-PCR (qRT-PCR) (B) analyses of the mature miRNA levels in the miR-17-92 cluster during HCMV Toledo infection (5 MOI). Total RNAs were prepared for analysis at the indicated time point. Error bars mean the standard errors (n=3).

A

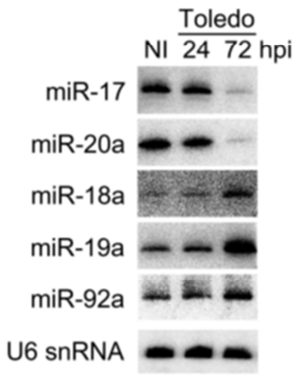
Toledo
NI 24 72 hpi
miR-17
miR-20a
miR-18a
miR-19a
miR-92a
U6 snRNA

B

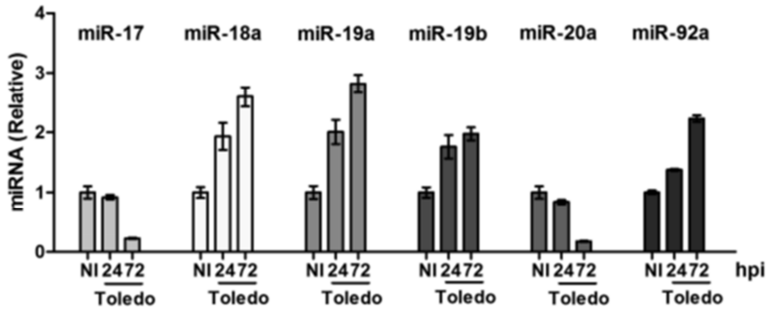
miR-17
miR-18a
miR-19a
miR-19b
miR-20a
miR-92a
miRNA (Relative)
0
1
2
3
4
NI 24 72
Toledo
hpi

Figure 8. Expression of miR-17 family during Toledo/ToledoΔ15kb infection

Northern blot analysis of miR-17, miR-20a, and miR-19a in HFFs infected with Toledo-WT or ToledoΔ15kb (5 MOI) at 72 hpi. U6 snRNAs were used as a loading control.

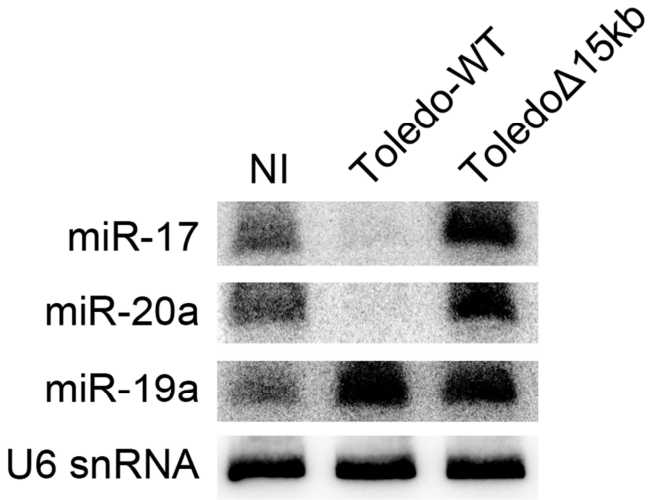
NI
Toledo-WT
ToledoΔ15kb
miR-17
miR-20a
miR-19a
U6 snRNA

Figure 9. miR-17-92 cluster expression during AD169 infection

(A, B) HFFs were infected with an attenuated strain AD169 or ToledoΔ15kb at 5 MOI. The RNA levels were quantified through qRT-PCR. (A) Fold-change of the mature miRNAs in the miR-17-92 cluster during infection. (B) Pri-miRNA levels of miR-17-92 during AD169 infection. The error bars represent ±1 SD.

A

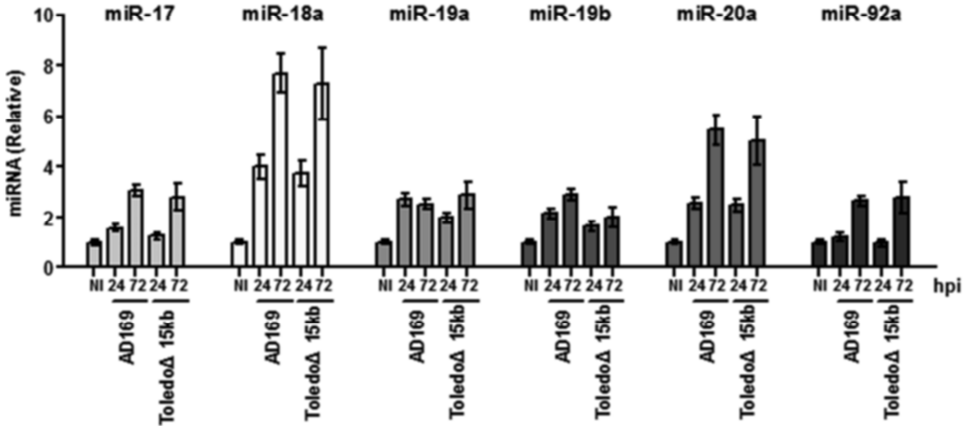
miR-17
miR-18a
miR-19a
miR-19b
miR-20a
miR-92a
miRNA (Relative)
10
8
6
4
2
0
NI 24 72 24 72
hpi
AD169
ToledoΔ 15kb

B

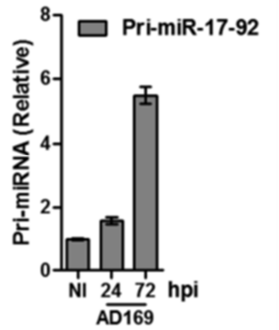
Pri-miR-17-92
Pri-miRNA (Relative)
8
6
4
2
0
NI 24 72 hpi
AD169

2. HCMV infection induced primary transcription of the miR-17-92 cluster, followed by the selective downregulation of mature miR-17 and miR-20a

The differential expression of individual miRNAs within the same miRNA cluster was surprising and unexpected. To further investigate the differential regulation of the miR-17-92 cluster, I examined whether Toledo affects the transcription of primary miR-17-92 (pri-miR-17-92). During Toledo infection, pri-miR-17-92 levels gradually increased at 72 hr postinfection (hpi) (Figure 10A), which has also been observed during ToledoΔ15kb infection (Figure 10B). Previous studies have reported that E2F family activates the transcription of the miR-17-92 cluster (Sylvestre et al., 2007), HCMV Immediate early protein 1 (IE1) interacts with E2F1 during infection (Margolis et al., 1995), and HCMV Immediate early protein 2 (IE2) increases the expression of E2F-response genes (Hagemeier et al., 1994; Song and Stinski, 2002); therefore, I hypothesized that HCMV IE1 and IE2 could be responsible for the observed upregulation of pri-miR-17-92 expression during Toledo infection. Indeed, the ectopic expression of either IE1 or IE2 increased the pri-miR-17-92 levels, and the coexpression of these proteins increased the induction of pri-miR-17-92 expression (Figure 11A). To

examine whether IE1 and IE2 elevate pri-miR-17-92 expression during infection, I generated siRNAs specific for IE1 and IE2. The siRNA-mediated knockdown of IE1 and/or IE2 inhibited the upregulation of pri-miR-17-92 (Figure 11B). These results indicate that HCMV IE1 and IE2 play a role in inducing primary miR-17-92 transcription.

Next, I investigated the mechanisms by which Toledo downregulates the levels of the mature forms of miR-17 and miR-20a. Northern blot analysis indicated that the precursor miRNAs (pre-miRNAs) of miR-17 and miR-20a are gradually increased during infection. In contrast to the results for pre-miRNA, the mature levels of miR-17 and miR-20a were dramatically reduced during infection (Figure 12). I quantified the miR-17* and miR-20a* levels using qRT-PCR analysis, revealing that the expression of these miRNAs was increased (Figure 13). These results demonstrate that Toledo initially induces the transcription of pri-miR-17-92 and selectively downregulates the miR-17 family (miR-17 and miR-20a) of the miR-17-92 cluster at the mature level.

Figure 10. Primary miR-17-92 levels during Toledo infection

(A and B) qRT-PCR results for the primary miR-17-92. HFFs were infected with either Toledo-WT or ToledoΔ15kb (5 MOI). At the indicated time, total RNAs were prepared for analysis. The primary miRNA levels were normalized by GAPDH mRNA levels.

A

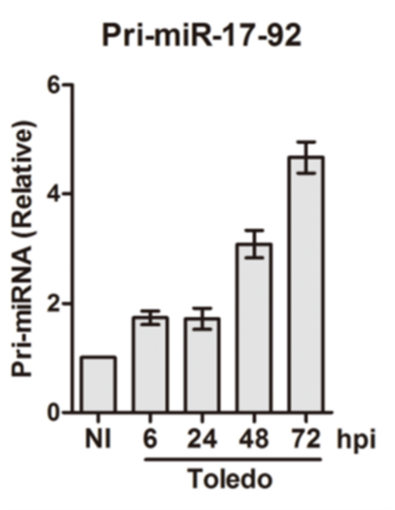
Pri-miR-17-92
Pri-miRNA (Relative)
6
4
2
0
NI
6
24
48
72
hpi
Toledo

B

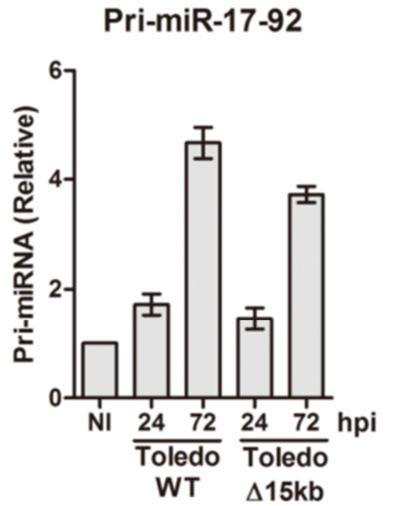
Pri-miR-17-92
Pri-miRNA (Relative)
6
4
2
0
NI
24
72
24
72
hpi
Toledo
WT
Toledo
Δ15kb

Figure 11. Functions of IE1/2 within miR-17-92 induction

(A) Using the adenoviral expression system, HCMV IE1 and IE2 were expressed in HFFs. Adenovirus containing the trans-activator gene (Ad-Trans) was used for the control infection. HFFs were infected with either adenovirus-IE1 (Ad-IE1) or adenovirus-IE2 (Ad-IE2) at 10 MOI. After 48 hr, the pri-miRNA was analyzed using qRT-PCR.

(B) The loss of function study of HCMV IE1 and IE2 for the induction of miR-17-92. HFFs were transfected with IE1 or IE2-specific siRNAs (final concentration, 20 nM) and subsequently infected with Toledo-WT (2 MOI). At 3 dpi, the infected cells were harvested to quantify the pri-miRNA transcripts. The anti-IE1 and anti-IE2 blots show the efficiency of IE1 and IE2 knockdown (right panel).

A

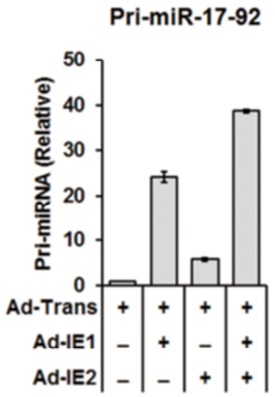
Pri-miR-17-92
Pri-miRNA (Relative)
50
40
30
20
10
0
Ad-Trans + + + +
Ad-IE1 – + – +
Ad-IE2 – – + +

B

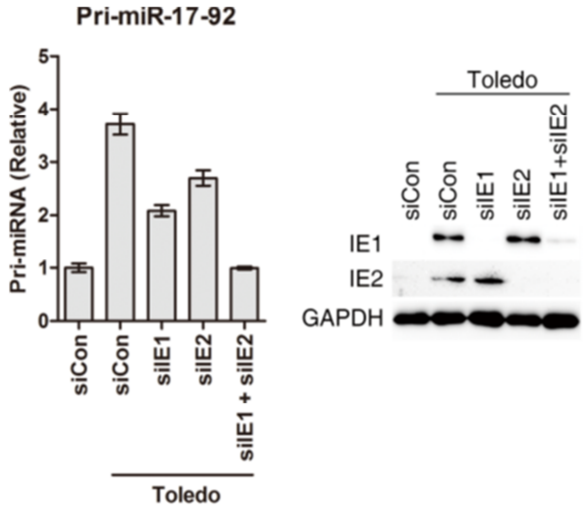
Pri-miR-17-92
Pri-miRNA (Relative)
5
4
3
2
1
0
siCon
siCon
siIE1
siIE2
siIE1 + siIE2
Toledo
Toledo
siCon
siCon
siIE1
siIE2
siIE1+siIE2
IE1
IE2
GAPDH

Figure 12. Expression of the precursor and mature form of miR-17 and miR-20a during Toledo infection

Northern blot analysis demonstrating the expression of the precursor and mature form of miR-17 and miR-20a during Toledo infection. U6 snRNA was used as a loading control. NI indicates the noninfected control.

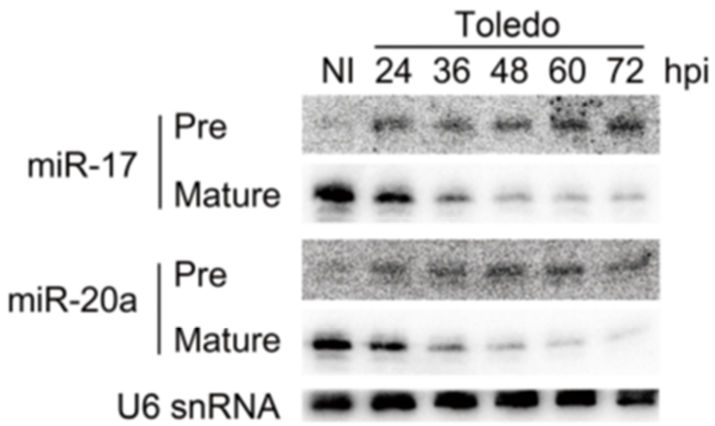
Toledo
NI 24 36 48 60 72 hpi
miR-17
Pre
Mature
miR-20a
Pre
Mature
U6 snRNA

Figure 13. miR-17* and miR-20a* expression during Toledo infection

HFFs were infected with Toledo at 5 MOI. The level of miRNA* was quantified through qRT-PCR. The error bars represent ±1 SD. miR-17* is also known as miR-17-3p. miR-20a* is also known as miR-20a-3p. The gene information of miRNAs is based on *miRBase*.

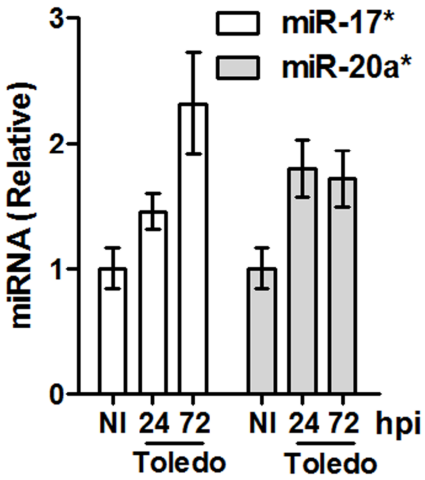
miR-17*
miR-20a*
miRNA (Relative)
3
2
1
0
NI 24 72 NI 24 72 hpi
Toledo
Toledo

3. HCMV clinical strain-specific RNA mediates the turnover of the miR-17 and miR-20a through sequence-specific RNA-miRNA interactions

To identify the viral factors involved in the selective degradation of miRNAs within the miR-17 family, I treated cells with either the transcriptional inhibitor actinomycin D (ActD) or the translational inhibitor cycloheximide (CHX). Both ActD and CHX treatments suppressed the upregulation of miR-19a by Toledo (Figure 14A, left), suggesting that the Toledo-mediated upregulation of miR-19a requires the synthesis of both RNA and protein. Interestingly, ActD, but not CHX, blocked the Toledo-induced reduction of miR-17 expression, suggesting that viral RNA is involved in mediating the downregulation of miR-17 (Figure 14A, right).

To identify the location of the regulatory elements within the 15kb-UL/b' region, I generated partial genomic clones of the 15-kb region to determine which clones could induce the degradation of miR-17 (Figure 15A). Clone 3 induced the downregulation of mature miR-17 when transfected into ToledoΔ15kb-infected HFFs (Figure 15B, left), without affecting pri-miR-17-92 levels (Figure 15B, right). A major polycistronic transcript of approximately 1.6 kb in length has been identified within the

3-kb region of clone 3 (He et al., 2011; Stern-Ginossar et al., 2012). This transcript (hereafter called UL144-145 RNA) contains the 5′UTR, the UL144 ORF, an intergenic region, the UL145 ORF, and 3′UTR sequences (Figure 16A) and exhibits “early” viral gene expression kinetics (Figure 14B). In Figure 14, I observed that the degradation phenotype of miR-17 was abolished in ActD-treated cells but not in CHX-treated cells. UL144-145 RNA was normally expressed in DMSO or CHX treated cells, but reduced UL144-145 RNA was observed in ActD-treated cells (Figure 14C). I also confirmed that UL144-145 RNA was expressed in Clone 3-transfected HFFs, and the expression level was comparable with that in Toledo-WT-infected cells (Figure 15C).

To determine the potential association between the viral RNA element and miRNA turnover (Figure 14), I examined whether the UL144-145 RNA element alone is sufficient to mediate miRNA turnover. Using the bioinformatics algorithm *RNA Hybrid*, I identified a favorable miRNA-binding site within the intergenic region of UL144-145 RNA (Figure 16B). An analysis of the secondary structure of the intergenic region of UL144-145 RNA using RNAfold software (Luxan et al.) showed that the miR-17 binding site of UL144-145 RNA comprises a bulged bipartite non-base-paired nucleotide sequence complementary to miR-17,

separated by 6 intramolecular base pairs (Figure 3B). The 3-dimensional structure model, constructed using the Rosetta program (Das and Baker, 2007), predicted that the 6-base pair duplex is bent inward, bringing the bipartite binding site together, creating a favorable structure for miR-17 binding (Figure 18). The overexpression of UL144-145 RNA in HEK293T cells resulted in the specific downregulation of miR-17 and miR-20a in a dose-dependent manner, and the miR-19a levels remained unchanged (Figure 16C).

These results suggested that the UL144-145 RNA mediates the decay of miR-17 and miR-20a. The mutated UL144-145 RNA, containing a triple-nucleotide substitution mutation in the miR-17 seed binding site, could no longer downregulate miR-17 and miR-20a (Figure 16D), demonstrating that UL144-145 RNA functions through sequence-specific interactions with miRNA. To further characterize the importance of sequence-specific interactions in the UL144-145 RNA-mediated degradation of miRNA, I determined whether UL144-145 RNA could be retargeted to other miRNA family members from the miR-17-92 cluster that were not subjected to Toledo-induced degradation. The UL144-145 RNA-binding site for miR-17 was replaced with the binding site for miR-18a. This mutant could effectively downregulate miR-18a, whereas it

could no longer target miR-17 and miR-20a for degradation (Figure 17A). Similarly, point mutations in the UL144-145 RNA complementary to the seed sequence of miR-92a resulted in the specific degradation of miR-92a (Figure 17B). Taken together, these data demonstrate that the UL144-145 RNA-mediated degradation of miRNAs occurs in a sequence-specific manner.

Figure 14. Drug-sensitivity assay

(A) Drug-sensitivity assay. At 12 hpi Toledo-WT (5 MOI), HFFs were treated with DMSO as a control, actinomycin D (ActD), or cycloheximide (CHX). After 36 hr, the total RNA from the HFFs was used for quantitative analysis.

(B-C) The expression of UL144-145 RNA was detected by RT-PCR. (B) Early phase expression of UL144-145 RNA. HFF cells were infected with Toledo at 5 MOI and treated with cycloheximide (100 ng/ml) or ganciclovir (50 μM) for 24 hr. Cells were pretreated with cycloheximide for 30 min prior to infection to completely block viral early gene expression. Ganciclovir was used to inhibit late gene expression by blocking viral replication. At 24 hpi, the total RNA from the infected cells was prepared for analysis. (C) UL144-145 RNA expression in the drug-treated cells. HFF cells were infected with Toledo at 5 MOI and at 12 hpi, HFFs were treated with DMSO, actinomycin D, or cycloheximide. After 36 hr, total RNA from the HFFs was prepared for analysis.

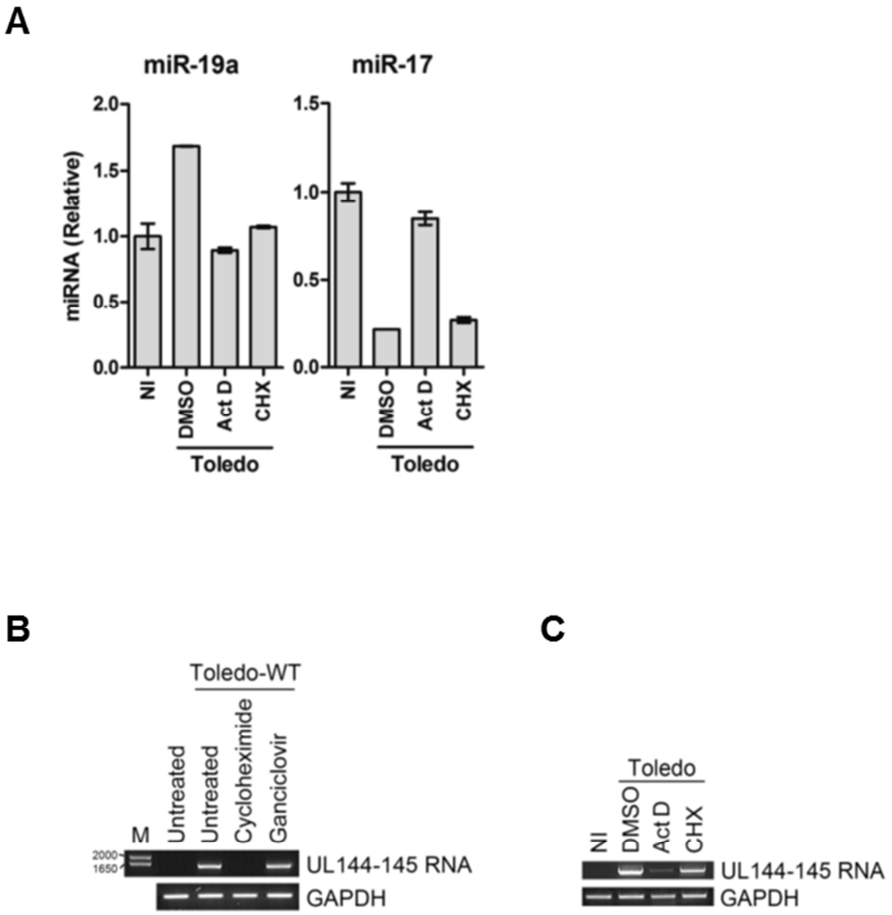
A
miR-19a
miR-17
miRNA (Relative)
2.0
1.5
1.0
0.5
0.0
NI
DMSO
Act D
CHX
Toledo
B
Toledo-WT
M
Untreated
Untreated
Cycloheximide
Ganciclovir
2000
1650
UL144-145 RNA
GAPDH
C
Toledo
NI
DMSO
Act D
CHX
UL144-145 RNA
GAPDH

Figure 15. Clone recovery test with ToledoΔ15kb

(A) Illustration of the recovery test. The partial genomic sequences of the 15-kb region were cloned into a promoterless vector (pBlueScript). HFFs were infected with ToledoΔ17Seed (5 MOI) and transfected with the partial genomic clones. (B) Mature miR-17 and pri-miR-17-92 transcript levels quantified using qRT-PCR. (C) UL144-145 RNA expression in the clone recovery experiment. Toledo-WT-infected cells were used as positive controls.

A

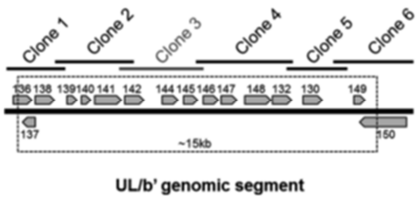
Clone 1
Clone 2
Clone 3
Clone 4
Clone 5
Clone 6
136 138 139 140 141 142 144 145 146 147 148 132 130 149
137
~15kb
150
UL/b' genomic segment

B

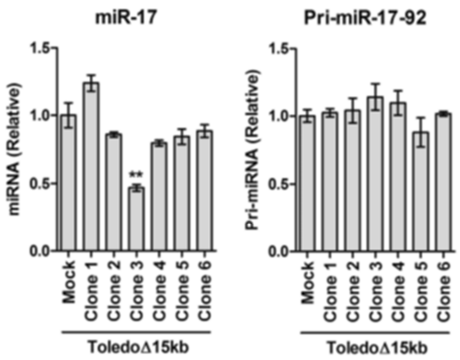
miR-17
Pri-miR-17-92
miRNA (Relative)
Pri-miRNA (Relative)
1.5
1.0
0.5
0.0
**
Mock
Clone 1
Clone 2
Clone 3
Clone 4
Clone 5
Clone 6
ToledoΔ15kb

C

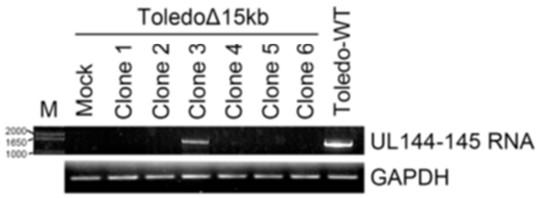
ToledoΔ15kb
M
Mock
Clone 1
Clone 2
Clone 3
Clone 4
Clone 5
Clone 6
Toledo-WT
2000
1650
1000
UL144-145 RNA
GAPDH

Figure 16. Identification of UL144-145 transcript as a decay factor of miR-17 family

(A) Schematic of the UL144-145 RNA locus in clone 3. The miR-17-binding site was mapped to the intergenic region between UL144 and UL145. (B) Two-dimensional representation for the intergenic region of UL144-145 RNA using *Mfold* software. Both the 5' and 3' complementary sequences to miR-17 (red) and the central bulge of the miR-17 binding site (blue) are indicated. (C) qRT-PCR detection of mature miRNA transcripts resulting from a dose-dependent transfection of HEK293T cells with UL144-145 RNA cloned into a pcDNA3.1 vector. (D) miRNA transcript levels of UL144-145 RNA with mutations in the miR-17 seed-binding site (UL144-145 seed mut). miRNA transcript levels of HEK293T cells transfected with the indicated constructs, as detected using qRT-PCR (** indicates $p < 0.01$; * indicates $p < 0.05$ by Student's *t*-test). NS represents nonspecific, and the error bars represent ±1 SD.

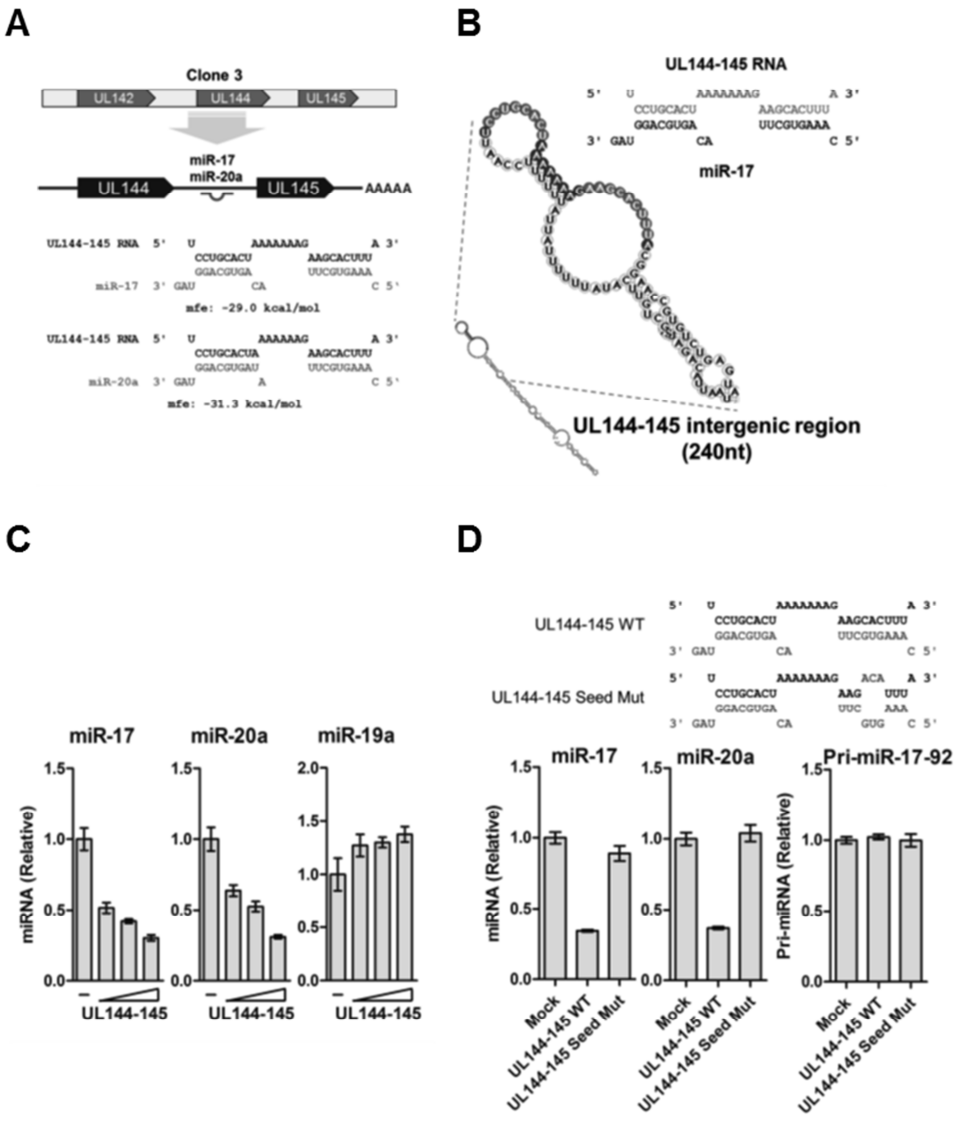
A
Clone 3
UL142
UL144
UL145
miR-17
miR-20a
UL144
UL145
AAAAA
UL144-145 RNA 5' U AAAAAAAG A 3'
CCUGCACU AAGCACUUU
GGACGUGA UUCGUGAAA
miR-17 3' GAU CA C 5'
mfe: -29.0 kcal/mol
UL144-145 RNA 5' U AAAAAAG A 3'
CCUGCACUA AAGCACUUU
GGACGUGAU UUCGUGAAA
miR-20a 3' GAU A C 5'
mfe: -31.3 kcal/mol
B
UL144-145 RNA
5' U AAAAAAAG A 3'
CCUGCACU AAGCACUUU
GGACGUGA UUCGUGAAA
3' GAU CA C 5'
miR-17
UL144-145 intergenic region
(240nt)
C
miR-17
miR-20a
miR-19a
miRNA (Relative)
1.5
1.0
0.5
0.0
2.0
1.5
UL144-145
UL144-145
UL144-145
D
UL144-145 WT
5' U AAAAAAAG A 3'
CCUGCACU AAGCACUUU
GGACGUGA UUCGUGAAA
3' GAU CA C 5'
UL144-145 Seed Mut
5' U AAAAAAAG ACA A 3'
CCUGCACU AAG UUU
GGACGUGA UUC AAA
3' GAU CA GUG C 5'
miR-17
miR-20a
Pri-miR-17-92
miRNA (Relative)
Pri-miRNA (Relative)
1.5
1.0
0.5
0.0
Mock
UL144-145 WT
UL144-145 Seed Mut

Figure 17. Retargeting UL144-145 to other miRNAs in miR-17-92 cluster

(A) Introduction of mutated binding sites into UL144-145. The miR-17 binding site of UL144-145 RNA was changed to a miR-18a-binding site (UL144-145 17→18a). (B) The miR-17 binding site of UL144-145 RNA was changed to a miR-92a binding site (UL144-145 17→92a). (A, B) miRNA transcript levels of HEK293T cells transfected with the indicated constructs, as detected using qRT-PCR (** indicates $p < 0.01$; * indicates $p < 0.05$ by Student's t-test). NS represents nonspecific, and the error bars represent ±1 SD.

A

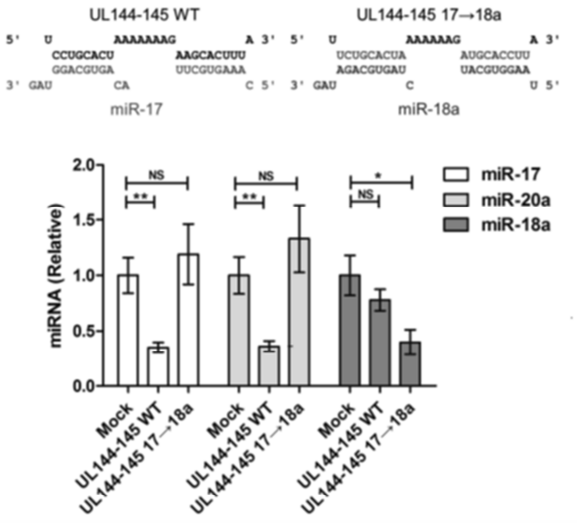
UL144-145 WT
UL144-145 17→18a
miR-17
miR-18a
miRNA (Relative)
miR-17
miR-20a
miR-18a
NS
**
*
Mock
UL144-145 WT
UL144-145 17→18a

B

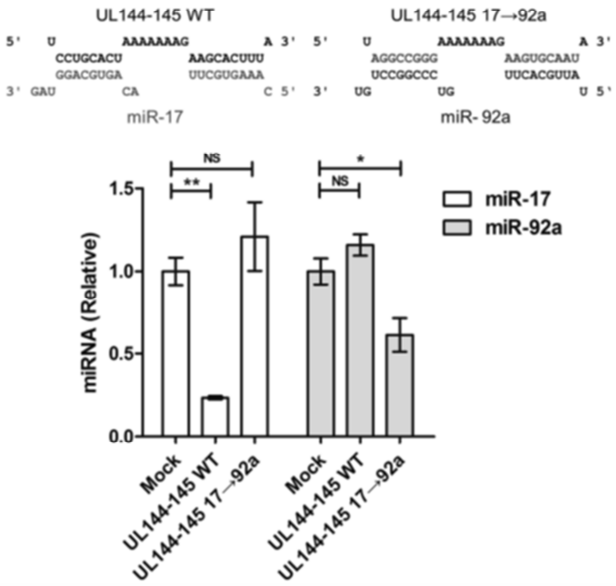
UL144-145 WT
UL144-145 17→92a
miR-17
miR- 92a
miRNA (Relative)
miR-17
miR-92a
NS
**
*
Mock
UL144-145 WT
UL144-145 17→92a

Figure 18. Predicted 3D RNA structure of UL144-145 intergenic region

Three-dimensional model structures of the intergenic region of UL144-145 RNA. Using Rosetta software, the 240-nt intergenic sequence of UL144-145 RNA was analyzed. Both 5' and 3' complementary sequences to miR-17 (red), the central bulge of miR-17 binding site (blue), and the 3' additional motif (orange) are shown.

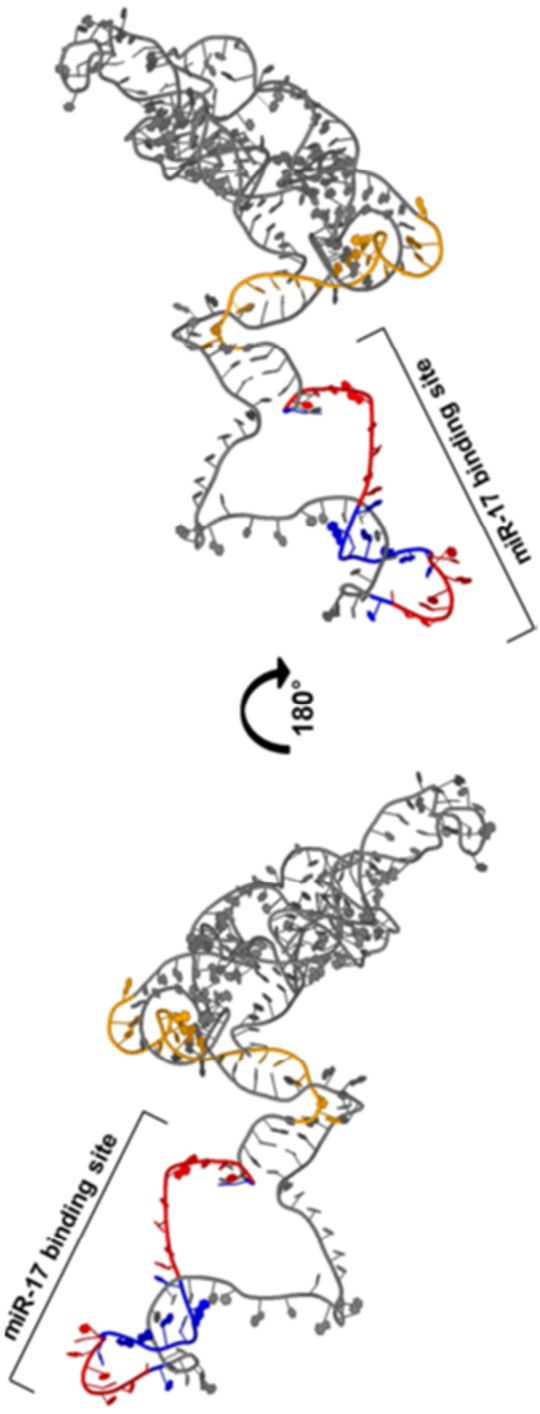
miR-17 binding site
180°
miR-17 binding site

4. Identification of a miRDE that directs the turnover of miRNA through non-canonical miRNA-mRNA interactions

To identify the core element required for the degradation of miR-17 family members and understand the nature of miRNA-target RNA interactions, I generated a series of firefly luciferase reporter constructs based on the 240-nt intergenic region harboring the miR-17 binding site (Figure 19A). Both the firefly-736nt and firefly-240nt constructs could downregulate the expression of miR-17 and miR-20a (Figure 19B), indicating that the 240-nt intergenic region of UL144-145 RNA is sufficient for the downregulation of the miR-17 family (sequence information in Figure 23). Notably, based on the luciferase activity of firefly-240nt observed in cells overexpressing miR-17 or miR-20a (Figure 20), I did not observe miR-17- or miR-20a-mediated targeting of firefly-240nt RNA, which is required for canonical miRNA-mRNA interactions.

These results demonstrated that opposite outcomes in miRNA or mRNA degradation depend on the nature of the miRNA-mRNA interactions. Firefly-30nt did not downregulate the miR-17 transcript level, indicating that the miR-17-binding sequence alone is not sufficient for inducing miR-17 turnover (Figure 19C). To identify the minimal

sequence for miR-17 degradation, I analyzed a series of deletion mutants and observed that the additional 20-nt (Δ3-2~Δ3-6 region) adjacent to the 30-nt miR-17 binding site was essential for miR-17 downregulation (Figure 21). Thus, this approximately 50-nt viral intergenic noncoding RNA region sequence represents the “miRNA decay element” (miRDE; miRDE sequence information in Figure 23).

To further validate the ability of miRDE to degrade miRNA and evaluate the use of miRDE as a tool for studying miRNA regulation, I generated a 50-mer RNA oligo (miRDE-50-mer_WT) to determine whether miRDE could serve as a short RNA oligomer. The expression of miR-17 was reduced in a dose-dependent manner in miRDE-transfected cells (Figure 22A) but not in cells transfected with the miRDE seed mutant (miRDE-50-mer_seed mut) containing a mutated miR-17 binding site (Figure 22B). The 30-mer RNA oligo (miRDE-30-mer), containing solely the miR-17 binding site, resulted in relatively inefficient downregulation (Figure 22C). These results indicate that the 50-mer viral intergenic noncoding RNA region sequence is essential and sufficient for regulating the miR-17 family and functions independently of mRNA context.

Figure 19. Intergenic region is sufficient to degrade miR-17 and miR-20a.

(A) Schematic of the construction of the following firefly luciferase reporter systems: firefly-736nt containing the intergenic region, UL145 ORF, and 3′UTR; firefly-240nt, containing only the intergenic region; and firefly-30nt, containing only the miR-17 binding site. (B) Overexpression of the reporter constructs in HEK293T. Fold-change in miR-17 and miR-20a, but not pri-miR-17-92, expression through Firefly-736nt and Firefly-240nt, detected using qRT-PCR. (C) Effects of firefly-30nt on miR-17 decay.

A


miR-17
miR-20a
UL144-145
UL144
UL145
Firefly
Firefly
Firefly-736nt
Firefly
UL145
Firefly-240nt
Firefly
Firefly-30nt
Firefly

B

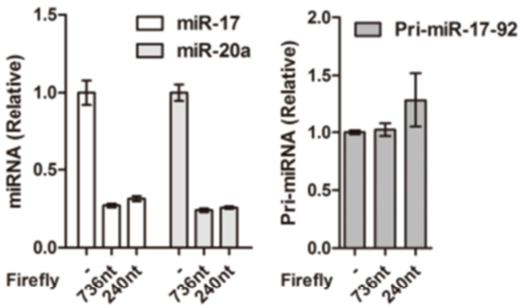
miR-17
miR-20a
miRNA (Relative)
1.5
1.0
0.5
0.0
Firefly
-
736nt
240nt
-
736nt
240nt
Pri-miR-17-92
Pri-miRNA (Relative)
2.0
1.5
1.0
0.5
0.0
Firefly
-
736nt
240nt

C

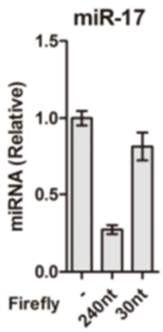
miR-17
miRNA (Relative)
1.5
1.0
0.5
0.0
Firefly
-
240nt
30nt

Figure 20. Non-canonical interaction between miR-17 family and UL144-145 intergenic region

miRNA targeting assay. HEK293T cells were cotransfected with Renilla luciferase, the firefly-240nt vector, and the indicated amount of miR-17 or miR-20a using liposomes. Twenty-four hr post-transfection, the luciferase activity of transfected cells was determined. The relative luciferase activity was calculated as the ratio of firefly to Renilla luciferase activity.

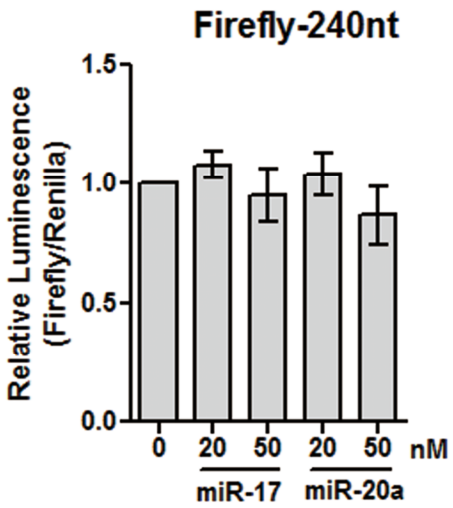
Firefly-240nt
Relative Luminescence
(Firefly/Renilla)
1.5
1.0
0.5
0.0
0
20
50
20
50
nM
miR-17
miR-20a

Figure 21. Deletion screening to identify the minimal requirement for miR-17 decay

(A) Schematic of the deletion screening of the UL144-145 intergenic region to identify the additional motif. (B) Primary screening with 40-nt scale deletion. (C) Secondary screening with 4-nt scale deletion in Δ3 region. (A-C) Synthetic RNA oligomers of the minimized viral intergenic RNA. The nucleotide sequences of miRDE RNA oligomers are shown in Figure 23. HEK293T cells were transfected with the indicated amount of RNA oligomers, and the total RNA was analyzed using qRT-PCR.

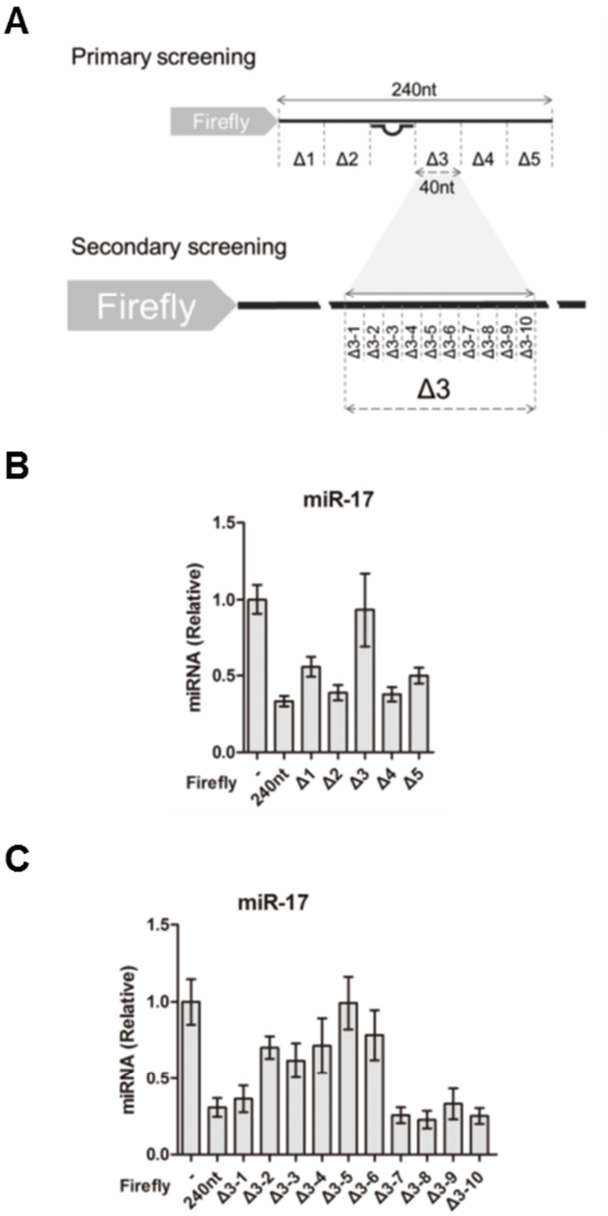
A
Primary screening
240nt
Firefly
Δ1
Δ2
Δ3
Δ4
Δ5
40nt
Secondary screening
Firefly
Δ3-1
Δ3-2
Δ3-3
Δ3-4
Δ3-5
Δ3-6
Δ3-7
Δ3-8
Δ3-9
Δ3-10
Δ3
B
miR-17
miRNA (Relative)
1.5
1.0
0.5
0.0
Firefly
-
240nt
Δ1
Δ2
Δ3
Δ4
Δ5
C
miR-17
miRNA (Relative)
1.5
1.0
0.5
0.0
Firefly
-
240nt
Δ3-1
Δ3-2
Δ3-3
Δ3-4
Δ3-5
Δ3-6
Δ3-7
Δ3-8
Δ3-9
Δ3-10

Figure 22. 50 nt RNA oligomers is sufficient to function as miR-17 decay element

(A) 50-nt RNA oligomer containing an miR-17-binding site and an additional 3′ additional motif in miRDE (miRDE-50-mer_WT). (B) miRDE wild-type oligomer (miRDE-50-mer_WT) or the miR-17 seed binding-site mutant oligomer (miRDE-50-mer_seed mut). (C) RNA oligomer containing the sole miR-17 binding site of miRDE (miRDE-30-mer). (A-C) The mature miRNA levels were quantified using qRT-PCR. The error bars represent ±1 SD.

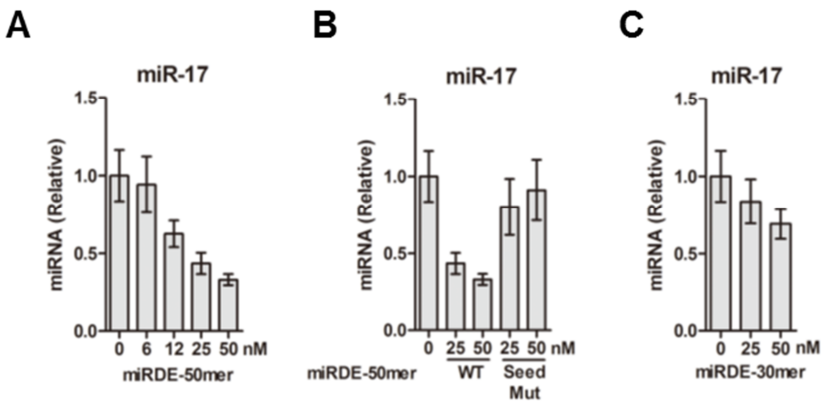
A
miR-17
miRNA (Relative)
1.5
1.0
0.5
0.0
0 6 12 25 50 nM
miRDE-50mer
B
miR-17
miRNA (Relative)
1.5
1.0
0.5
0.0
0 25 50 25 50 nM
miRDE-50mer
WT
Seed Mut
C
miR-17
miRNA (Relative)
1.5
1.0
0.5
0.0
0 25 50 nM
miRDE-30mer

Figure 23. miRDE (miRNA Decay Element) in HCMV genome

Genomic sequences of the intergenic region in UL144-145 RNA. The sequences were obtained from GenBank (GU937742.1). The miR-17 binding site (upper grey) and the additional 3′ motif (lower grey) are shown using colored text.

UL144-145 240nt

GCTTCCTGTTGTTGTTTTTACATCACGGTACGATGAAGTC
ACACAGATAATTACAGATGAGCTGTTCATATTTTTTATTA
TTTTTTCCAATTCCTGCACTAAAAAAAGAAGCACTTTACG
GAACCGTGTCTGAGTATCTGTGGGGAATTTAGGTACTTTT
TGCCGACGTCAGGAAAAATAAGCTGTCGCCTACATAAGAG
CCCGGTGCTATCGTGCTGTCACTCTTTCTTGTTGCCTTCG

miR-17 binding site
3’ additional motif

5. miR-17 binding-site mutant HCMV loses the ability to differentially regulate the miR-17-92 cluster

I observed that the viral intergenic RNA sequence mediates the selective turnover of miR-17 and miR-20a, using an expression vector or RNA oligomer. To further investigate miRDE-mediated miRNA regulation during viral infection, I generated a Toledo mutant virus with a triple-nucleotide substitution mutation in the miRDE seed-binding site for miR-17 (ToledoΔ17Seed) and its revertant virus (Toledo-Rev) (Figure 24A). The expression of mature miR-17 and miR-20a was reduced in Toledo-WT and Toledo-Rev-infected cells, whereas the expression of these miRNAs was significantly increased in ToledoΔ17Seed-infected cells (Figure 24B). The levels of the precursor miR-17 and miR-20a transcript increased in all 3 viruses during infection (Figure 24B), and the pri-miR-17-92 and UL144-145 transcript levels were similar between these viruses (Figures 24C and D). Next, using a pulse-chase experiment with synthetic miR-17 duplexes, I examined whether the miRDE of Toledo could destabilize the mature miR-17. Prior to the experiment, I verified that the amount of exogenous miR-17 is much higher than the amount of endogenous miR-17 (Figure 25B). After HFFs were infected with mock, Toledo-WT or ToledoΔ17Seed and transfected with the miR-

17/miR-17* duplex, I monitored the levels of miR-17 as a function of time. The Toledo-WT-infected cells exhibited higher rates of exogenous miR-17 degradation than the mock or ToledoΔ17Seed-infected cells (Figure 25A). These results indicate that miRDE facilitates the degradation of mature miR-17 in the context of viral infections. I also investigated whether the degradation of miR-17 family is dependent on a specific Argonaute protein. I designed specific siRNAs targeting members of the Argonaute family (siAgo1, siAgo2, siAgo3 and siAgo4). Prior to the HCMV Toledo infection, HFF cells were treated with the specific siRNAs for 2 days, and the miR-17 levels were assessed at 48 hpi. The degradation of miR-17 during infection was not affected by the specific knockdown of Ago genes (Figure 26), suggesting that the decay of miR-17 during infection is not dependent to specific Ago protein.

Figure 24. A Mutant virus with triple base substitution in the miR-17 binding site

(A) Schematic of the miR-17 binding site mutant virus (ToledoΔ17Seed). Mutated residues in the miR-17-binding site are shown (CAC→ACA, red). (B-D) HFFs were infected with Toledo-WT, ToledoΔ17Seed, or Toledo-Rev (2 MOI). The infected cells were harvested at the indicated times and the total RNA was analyzed. (B) Northern blots showing the expression levels of the pre-miR-17 (top panel), the mature miR-17 (second panel), the pre-miR-20a (third panel), and the mature miR-20a (fourth panel). (C) Pri-miR-17-92 levels quantified using qRT-PCR. (D) Levels of UL144-145 transcripts detected using qRT-PCR.

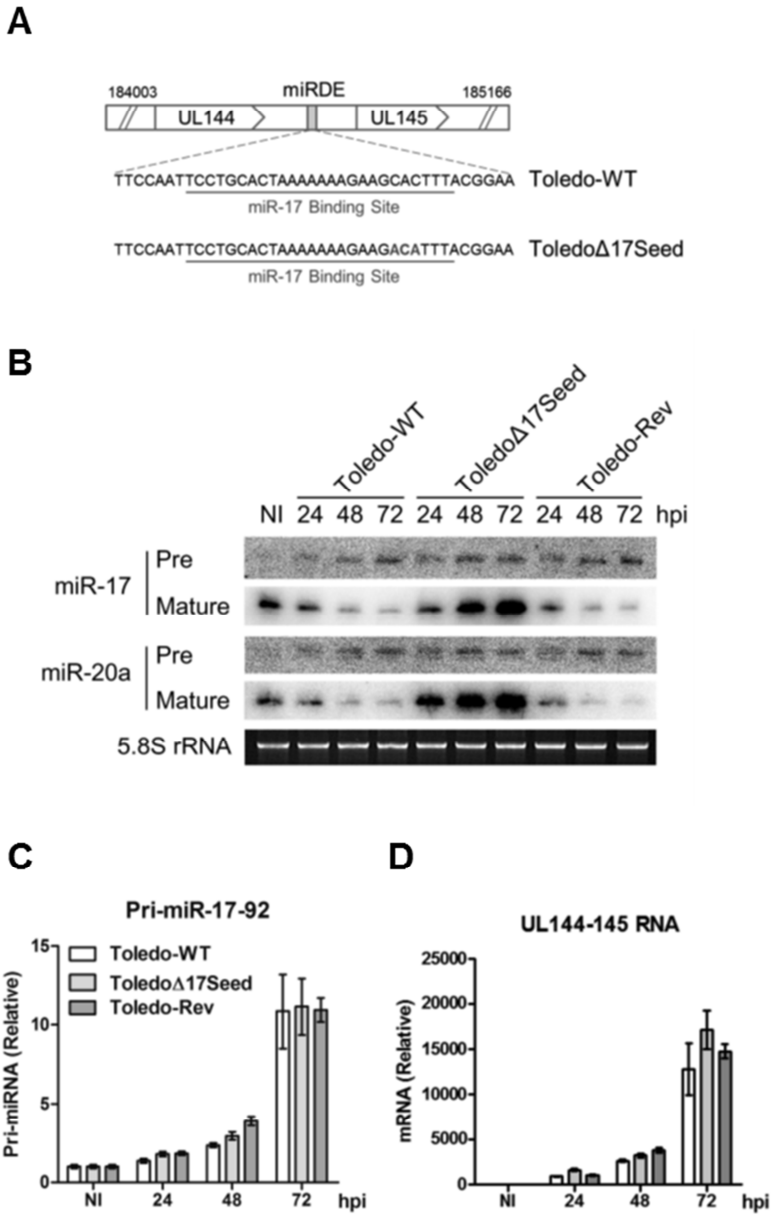
A
184003
miRDE
185166
UL144
UL145
TTCCAATTCCTGCACTAAAAAAAGAAGCACTTTACGGAA
Toledo-WT
miR-17 Binding Site
TTCCAATTCCTGCACTAAAAAAAGAAGACATTTACGGAA
ToledoΔ17Seed
miR-17 Binding Site
B
Toledo-WT
ToledoΔ17Seed
Toledo-Rev
NI 24 48 72 24 48 72 24 48 72 hpi
miR-17
Pre
Mature
miR-20a
Pre
Mature
5.8S rRNA
C
Pri-miR-17-92
Toledo-WT
ToledoΔ17Seed
Toledo-Rev
Pri-miRNA (Relative)
15
10
5
0
NI
24
48
72
hpi
D
UL144-145 RNA
mRNA (Relative)
25000
20000
15000
10000
5000
0
NI
24
48
72
hpi

Figure 25. miRNA stability assay with WT or mutant virus infection

(A) Stability of mature miRNA during HCMV infection, determined using pulse-chase assays. qRT-PCR was used to measure the abundance of miR-17 transcripts at the indicated time points after transfection with synthetic miR/miR* duplex, and 0.2 nM of the miR-17/miR-17* duplex was transfected. The error bars represent ±1 SD.

(B) Northern blot analysis of HFFs transfected with the indicated amount of miR-17/miR-17* duplex over a 4 hr incubation period. The transfected cells were washed with PBS and harvested for analysis. The expression levels of miR-18a were used as a negative control.

A

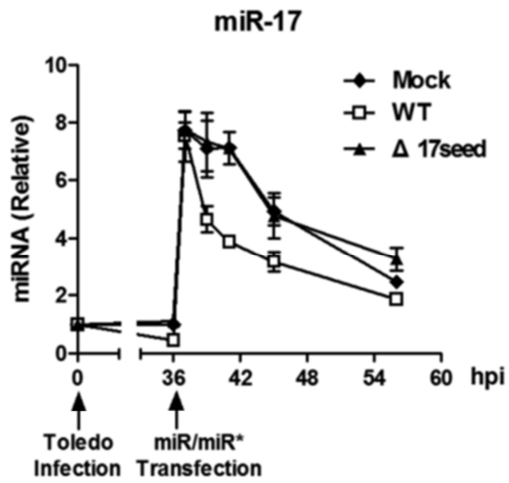
miR-17
Mock
WT
Δ 17seed
miRNA (Relative)
10
8
6
4
2
0
0
36
42
48
54
60
hpi
Toledo Infection
miR/miR* Transfection

B

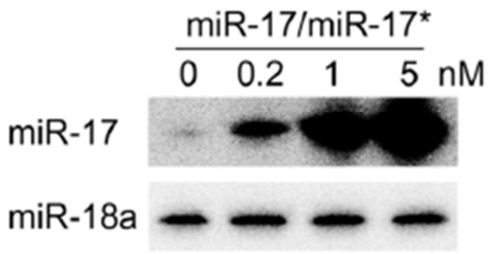
miR-17/miR-17*
0 0.2 1 5 nM
miR-17
miR-18a

Figure 26. Knock-down effect of a specific Ago on the miRDE-mediated miR-17 decay

HFFs were transfected with specific siRNA targeting Ago family. At 2 days after transfection, Toledo-WT or Toledo Δ17Seed were infected at 5 MOI, and a second siRNA transfection was performed for the efficient knockdown of Ago. At 48 hpi, the infected cells were harvested for RNA analysis. The knockdown efficiency of each Ago was determined using specific qRT-PCR. The error bars represent ±1 SD.

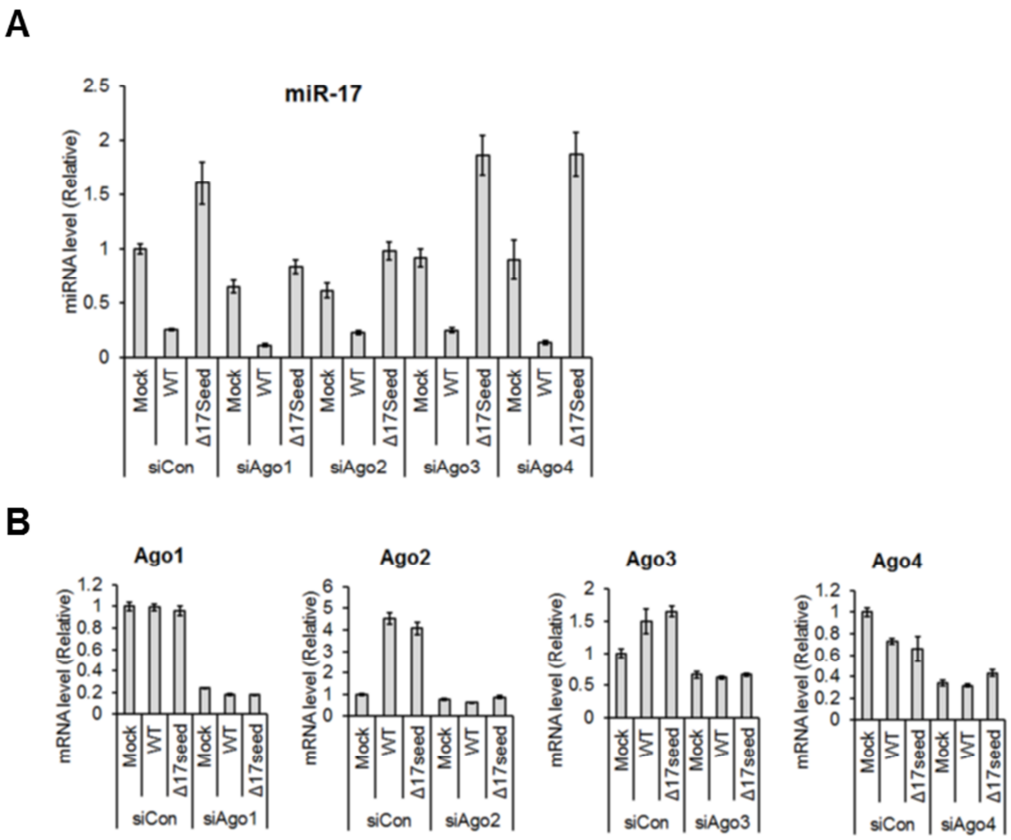
A
miR-17
miRNA level (Relative)
2.5
2
1.5
1
0.5
0
Mock
WT
Δ17Seed
siCon
siAgo1
siAgo2
siAgo3
siAgo4
B
Ago1
Ago2
Ago3
Ago4
mRNA level (Relative)
Mock
WT
Δ17seed
siCon
siAgo1
siAgo2
siAgo3
siAgo4

6. miRDE-mediated regulation of the miR-17 family accelerates virus production

To determine the physiological relevance of these observations, I assessed the effects of the miRDE-mediated regulation of miR-17 on viral lytic growth after infecting HFFs with Toledo-WT or ToledoΔ17Seed at an MOI of 2. Interestingly, at early viral infection, ToledoΔ17Seed-infected HFFs showed less viral production than Toledo-WT-infected HFFs. Virus production was 80-, 40- and 4-fold reduced at 2, 3 and 4 dpi in ToledoΔ17Seed-infected cells compared with that in Toledo-WT-infected cells. The viral production in Toledo-WT and ToledoΔ17Seed-infected cells reached a plateau at 5 dpi, presumably due to adverse environmental conditions (Figure 27A). The synthesis of the viral genome in ToledoΔ17Seed-infected cells was delayed and reduced (Figure 27B). ToledoΔ17Seed-infected cells showed partially reduced viral gene expression at 2 dpi, but the viral gene expression at 3–4 dpi was largely similar to that of Toledo-WT-infected HFFs (Figure 27C). Because miR-17 targets apoptotic genes, I used an Annexin-V assay to measure apoptosis during Toledo-WT or ToledoΔ17Seed infection in HFFs. The rate of apoptosis was low and similar in Toledo-WT- and ToledoΔ17Seed-infected cells (Figure 28).

I designed a rescue experiment using an anti-sense oligomer against miR-17 and miR-20a during infection. The specific anti-sense inhibitor against miR-17 and miR-20a significantly rescued the viral growth of ToledoΔ17Seed to a degree comparable with the growth of Toledo-WT (Figure 6D). Consistent with these results, ToledoΔ15kb produces infectious viruses at 1 day later than the parental viruses, with delayed growth rates (Wang et al., 2005), suggesting that miR-17 dysregulation could cause the growth delay of ToledoΔ15kb. Taken together, these data show that the degradation of miR-17 family accelerates viral production during HCMV infection. The functional importance of miRDE-mediated regulation of the miR-17 family within the miR-17-92 cluster might be supported through miRDE sequence conservation in all HCMV clinical isolates (Figure 6E). An analysis of the 4.2-kb genomic region encoding UL142 to UL147 from 14 HCMV clinical strains showed that the intergenic region harboring miRDE shows a remarkably high degree of sequence conservation. Particularly, the miR-17-binding sites are completely conserved in all HCMV clinical strains, suggesting the evolutionary adaptation of viruses to counteract cellular miRNA regulation.

Figure 27. Degradation of miR-17 by miRDE is essential for the rapid viral production during lytic infection

(A-C) HFFs were infected with Toledo-WT and ToledoΔ17Seed at 2 MOI. (A) Growth curves of Toledo-WT and ToledoΔ17Seed. The titer of cell-free virus in the supernatants of infected cultures was determined using limiting dilution analyses. (B) The levels of viral genomic DNA in HCMV-infected cells were determined using qPCR. The error bars represent ±1 SD. (C) Immunoblot analysis for the detection of HCMV immediate early proteins (IE1 and IE2) and late (gB) genes. (D) Rescue experiment using an anti-sense oligomer against miR-17 and miR-20a during Toledo infection. At 1 dpi, 100 nM of anti-sense oligomers were transfected to the infected HFFs. The cell-free virus in the supernatant was harvested at the indicated times for titration. A/S Con, anti-sense Control; A/S miR-17, anti-sense miR-17; A/S miR-20a, anti-sense miR-20a.

A

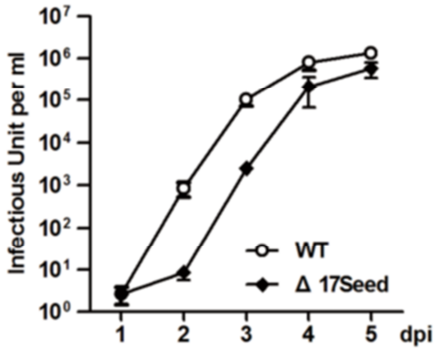
Infectious Unit per ml
10^7
10^6
10^5
10^4
10^3
10^2
10^1
10^0
WT
Δ 17Seed
1
2
3
4
5
dpi

B

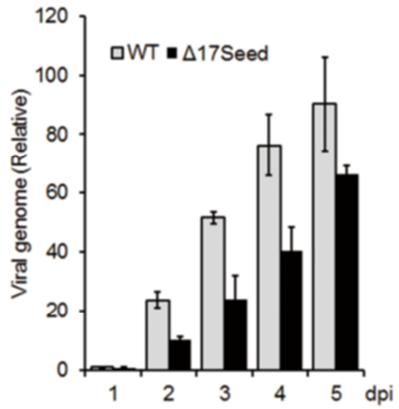
Viral genome (Relative)
120
100
80
60
40
20
0
WT ■ Δ17Seed
1
2
3
4
5
dpi

C

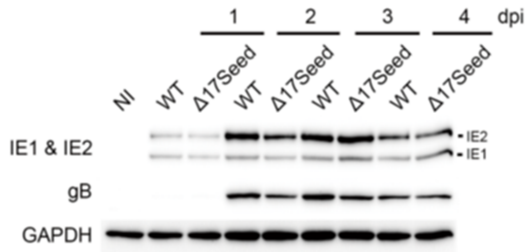
1
2
3
4
dpi
NI
WT
Δ17Seed
WT
Δ17Seed
WT
Δ17Seed
WT
Δ17Seed
IE1 & IE2
IE2
IE1
gB
GAPDH

Figure 28. Apoptosis rate during Toledo-WT and ToledoΔ17Seed infection

The percentage of apoptotic cells was determined through Annexin V staining and flow cytometry. HFFs were infected with Toledo-WT or ToledoΔ17Seed at 2 MOI. The error bars represent ±1 SD.

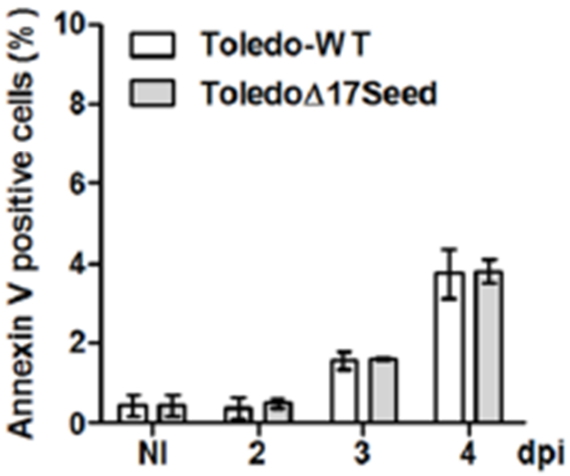
Annexin V positive cells (%)
10
8
6
4
2
0
Toledo-WT
ToledoΔ17Seed
NI
2
3
4
dpi

Figure 29. Rescue experiment using an anti-sense oligomer against miR-17 and miR-20a during Toledo infection

At 1 dpi, 100 nM of anti-sense oligomers were transfected to the infected HFFs. The cell-free virus in the supernatant was harvested at the indicated times for titration. A/S Con, anti-sense Control; A/S miR-17, anti-sense miR-17; A/S miR-20a, anti-sense miR-20a.

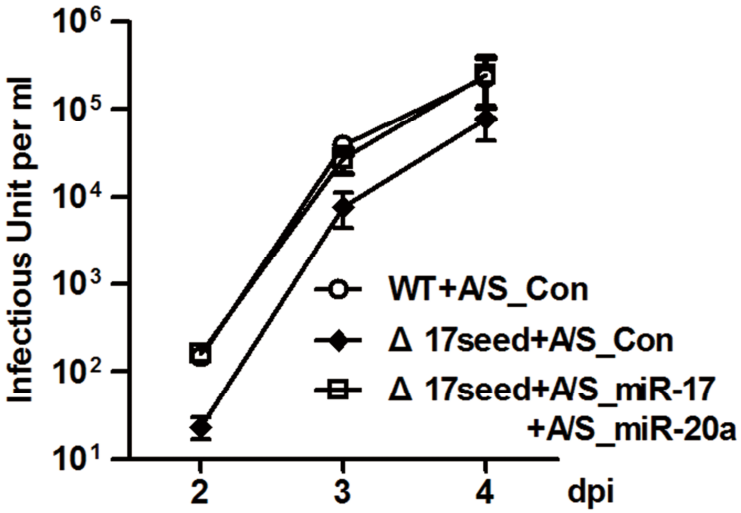
Infectious Unit per ml
10^6
10^5
10^4
10^3
10^2
10^1
2
3
4
dpi
WT+A/S_Con
Δ 17seed+A/S_Con
Δ 17seed+A/S_miR-17
+A/S_miR-20a

Figure 30. Sequence comparison of miRDE in the UL144-145 intergenic region of HCMV clinical isolates

The conserved (red) and nonconserved sequences (blue) are shown. The sequence of the miRNA decay element (miRDE) is boxed, and within the box, the sequences of the miR-17 binding site and 3′ additional motif have been noted.

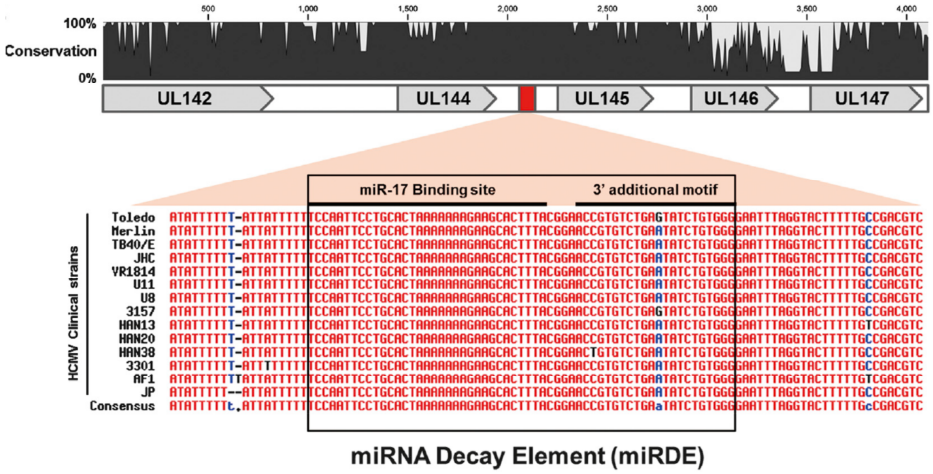

miRNA Decay Element (miRDE)

Figure 31. Schematic summary

Summary of HCMV clinical strain-mediated host miRNA regulation. Individual miRNAs in miR-17-92 cluster are differentially regulated at multiple steps. Non-canonical miRNA:mRNA interaction is highlighted in red box.

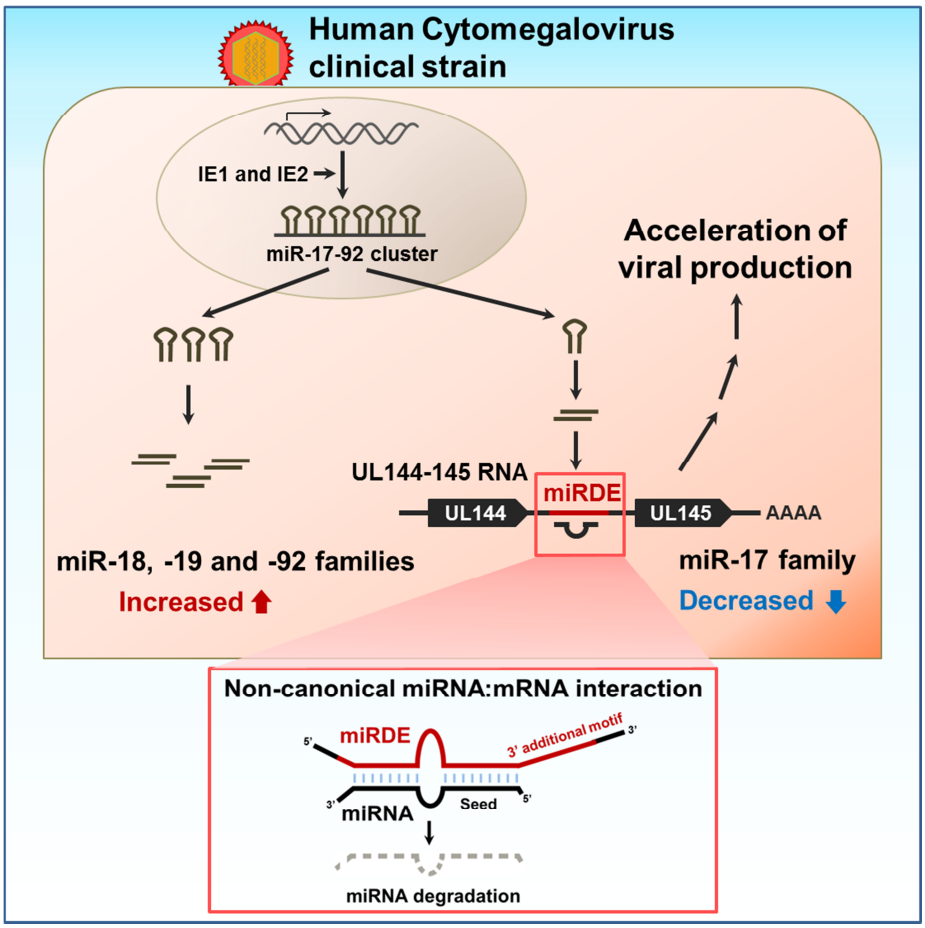
Human Cytomegalovirus
clinical strain
IE1 and IE2
miR-17-92 cluster
Acceleration of
viral production
UL144-145 RNA
miRDE
UL144
UL145
AAAA
miR-18, -19 and -92 families
Increased
miR-17 family
Decreased
Non-canonical miRNA:mRNA interaction
miRDE
3' additional motif
miRNA
Seed
miRNA degradation

IV. DISCUSSION

An intriguing aspect of this study is that the HCMV clinical strain regulates the host miR-17-92 cluster differentially and temporally by manipulating multiple steps of miRNA biogenesis during infection. I demonstrated that a 50-nt miRNA decay element (miRDE), comprising viral intergenic noncoding RNA region sequences, was specific for clinical strains and conserved in all HCMV clinical isolates. This miRDE was sufficient to induce the selective degradation of the miRNAs of the miR-17 family and other miRNAs via target site replacement. When the degradation of miR-17 through miRDE was abrogated, delayed HCMV production during lytic infection was observed, supporting the physiological relevance of miRDE-mediated miR-17 decay.

HCMV is predicted to contain over 250 ORFs (Murphy et al., 2003; Stern-Ginossar et al., 2012). Most viruses have evolved diverse strategies to maximize the coding capacity in a compact genome size. For example, many HCMV genes are transcribed as a polycistron. The ORFs in a polycistron use a common promoter element or poly-adenylation signal (Ma et al., 2012). HCMV cDNA library screening showed that 45% of the RNA transcribed from the HCMV genome was noncoding (Zhang et

al., 2007). Surprisingly, almost half of the transcribed RNA represents noncoding RNAs, raising a question about the functional roles of these noncoding RNAs. The polycistronic transcript UL144-145 RNA encodes the UL144 and UL145 ORFs and a 240-nt intergenic noncoding sequence. Thus, UL144-145 RNA exhibits features of both coding and noncoding RNA. The UL144 ORF encodes a homolog of the tumor necrosis factor receptor (TNFR) superfamily and facilitates HCMV immune surveillance evasion (Poole et al., 2006). The UL145 ORF encodes a polypeptide (Stern-Ginossar et al., 2012) with an as yet unknown function (Wang et al., 2011).

In this study, I identified the 50-mer-core sequence within intergenic RNA as a miRNA decay element (miRDE). The miRDE alone was sufficient to mediate the degradation of the miR-17 family within the miR-17-92 cluster. Furthermore, the miRDE could be retargeted to other miRNAs when the binding site for the miRNA of interest was appropriately replaced. Based on these observations and the predicted secondary structure of the 240-nt intergenic RNA sequences containing miRDE (Figure 16), I propose that the function of miRDE is likely to require the unpaired structure of miRNA-binding site. The 3' additional motif of miRDE was necessary for the efficient downregulation of miR-

17 family. This additional 3' motif might be involved in the recruitment of trans-factors, such as ribonuclease and RNA binding proteins. Alternatively, this motif might provide a rigid structural framework required for miRDE function. This virus-derived miRDE might be useful as a research tool and in therapeutics. Evidence, albeit limited, suggests that viruses use their own RNA to regulate host miRNAs. The noncoding RNA HSUR1 of *Herpesvirus saimiri* (Cazalla et al., 2010) and the 1.7-kb m169 transcript of murine cytomegalovirus (Libri et al., 2011; Marcinowski et al., 2012) mediate the degradation of the mature miR-27. Based on these studies and the results obtained here, I speculate that the cellular noncoding RNA genome also plays a role in regulating the turnover of mature miRNAs.

Why would HCMV have evolved a miR-17 degradation mechanism during lytic infection? In the present study, the downregulation of miR-17 accelerated viral production during lytic infection in fibroblasts. During lytic infection, the mutant virus, ToledoΔ17Seed, delayed viral production (after approximately 1 day) and genome synthesis. Accelerated viral growth could provide a fitness advantage. Previous studies on RNA viruses have shown that small increases in the rate of replication are sufficient to exclude other competitor strains, even when

the increases are marginal (Nowak and May, 2000). A recent study has provided evidence that HCMV gains a fitness advantage by accelerating IE2 expression, without amplifying the final expression levels, and rapid viral lytic cycles resulting from accelerated IE2 expression play a role in outcompeting nonaccelerated virus, leading to dominant growth (Teng et al., 2012).

These studies indicate that the accelerated growth of HCMV by miR-17 downregulation might contribute to virus fitness during lytic infection. Considering the remarkably broad cell tropism of HCMV *in vivo* (Sinzger et al., 2008) and the host innate-defense or inflammatory response, the accelerated viral production could be advantageous during *in vivo* clinical infection. The miR-17 family targets apoptotic and cell-cycle related genes (Olive et al., 2010). Toledo-WT and ToledoΔ17Seed induced similar and low levels of apoptosis during infection (Figure 28). This observation is not surprising because HCMV encodes several anti-apoptotic viral genes, such as UL37x1, UL36, UL38, IE1 and IE2 (McCormick, 2008). These redundant viral anti-apoptotic genes could potentially regulate apoptosis during Toledo-WT or ToledoΔ17Seed infection. Thus, the enhanced growth of the clinical isolate Toledo-WT is not solely due to blocking the anti-apoptotic function of miR-17.

Given that the cell-cycle regulators in S phase, such as E2F1, E2F2 and p21, are also targets of miR-17 (Olive et al., 2010), the delayed viral growth of ToledoΔ17Seed might be associated with cell-cycle arrest, consistent with the observation that the delayed viral growth correlated with the reduced synthesis of viral DNA genome (Figure 27). The physiological functions of the increased levels of miRNAs of miR-17-92 (miR-18a, miR-19a/b, and miR-92a) have not been explored. Because IE1 and IE2 block apoptosis during infection (Zhu et al., 1995) and miR-19 and miR-92 target the apoptotic genes Pten and Bim (Olive et al., 2010), I expect that the anti-apoptotic function of IE1 and IE2 might be associated with miR-17-92 cluster induction.

One of the important features of miRNA is its clustering propensity. One-third of human miRNAs are likely encoded within polycistronic miRNA clusters (Altuvia et al., 2005). Most studies on clustered miRNAs focus on elucidating the coordinated function and expression of miRNAs in a cluster. Previous studies on the oncogenic properties of miR-17-92 have shown that the component miRNAs of miR-17-92 cooperate to induce tumorigenesis (Mendell, 2008). In the present study, I observed that HCMV differentially regulates the expression of the host miRNA cluster, miR-17-92, through the manipulation of multiple steps in miRNA

expression, suggesting that a single miRNA cluster could generate multiple miRNA compositions upon receiving a specific stimulus. miR-17-92 is a well-characterized oncogenic miRNA. The sequences of the 6 mature miRNAs are highly conserved in all vertebrates, and these miRNAs play critical roles in the development of organs and cancer (Olive et al., 2010). However, the molecular mechanisms underlying the pleiotropic effects of these molecules remain unclear. These results provide insights into the differential regulation of miRNA clusters and will be helpful in future studies for determining the roles of these miRNAs in human disease.

V. EXPERIMENTAL PROCEDURES

Cells and viruses

Human embryonic kidney 293T (HEK293T) cells were maintained in DMEM medium (HyClone) containing 7.5% fetal bovine serum (FBS) (HyClone), 2 mM L-glutamine, 50 U/mL of penicillin, and 50 μg/mL of streptomycin. Human foreskin fibroblasts (HFFs) (ATCC, passages 10–15) were grown in DMEM supplemented with 10% FBS. Bacterial artificial chromosomes (BACs) of Toledo, ToledoΔ15kb, and AD169 were introduced into HFFs using electroporation (Gene-Pulser II, Bio-Rad). After 2 weeks, the culture supernatants were collected and titrated as infectious units after measuring the IE1-positive cells via immunofluorescence assays. Anti-IE1 (MAB810R, Millipore) and anti-gB (1-M-12, Santa Cruz Biotechnology) antibodies were used for the immunoblotting analyses. Adenoviruses expressing HCMV IE-1 (Ad-IE1) and IE2 (Ad-IE2) were provided from Jin-Hyun Ahn. Actinomycin D (A9415) and cycloheximide (C4859) were purchased from Sigma.

miRNA microarray

miRNA microarray experiments were performed to determine cellular miRNA expression during HCMV infection. Total RNAs from the uninfected control, Toledo-WT and ToledoΔ15kb-infected HFFs were isolated using TRIzol reagent (Invitrogen). Each sample was prepared according to the Agilent miRNA Microarray System protocol. The microarray data were deposited in NCBI-GEO under accession number GSE43761.

Firefly reporter construction and dual luciferase assay

I used pGL3-CMV (Promega), a firefly luciferase vector containing a CMV promoter, to analyze the biological functions of UL144-145 RNA and pRL-TK (Promega), a *Renilla* luciferase vector, to serve as a control reporter. The primers used in the reporter constructs are listed in Table 2. For miRNA targeting assay, HEK293T cells (1×10^5 cells in 24 well plate) were co-transfected with 1 ng of the firefly-240nt, 5 ng of *Renilla* luciferase vector and 50nM miRNA by Lipofectamin (Invitrogen). 24 hr later, firefly luciferase activity was normalized to *Renilla* luciferase activity. The firefly and *Renilla* luciferase activities were determined

according to manufacturer's instructions (Dual-Luciferase Reporter Assay System, Promega) using a luminometer (Berthold Technologies).

Northern blot and qRT-PCR

The miRNA sequences in this study were obtained from *miRBase* (Sanger Institute). The probes used for blotting miRNA were designed according to the sequence database. Total RNAs from HFFs and HEK293T cells were isolated using TRIzol reagent (Invitrogen). The total RNA was resolved on a gel containing 15% acrylamide and 8 M urea, transferred onto a nylon membrane (Zeta-probe GT, Bio-Rad), and EDC cross-linked for 1 hr (Pall and Hamilton, 2008). Hybridization was performed in a hybridization solution (Clontech) for 3 hr at 37°C, and the FUJI BAS film was exposed for 1 d. Total RNA was subsequently reverse transcribed with oligo-dT using M-MLV reverse transcriptase (Invitrogen) for 1 hr at 37°C and PCR-amplified using the iQ SYBR Green Supermix (Bio-Rad). The expression levels for the pri-miRNAs and target mRNAs were normalized to GAPDH mRNA expression levels. The cellular miRNAs were quantified through qRT-PCR using the miRNA assay kit (Taqman). Mature miRNAs were normalized to U6

snRNA.

Transfection of small RNA and plasmid DNA

Small RNAs (i.e., RNA oligomers, siRNAs and miRNA inhibitors) were transfected using the Dharmafect 1 reagent (Dharmacon). Twenty-four hr prior to transfection, HFFs and HEK293T cells were seeded onto a 12-well culture plate in the appropriate complete growth medium without antibiotics. The small RNAs and Dharmafect mixture were added into the culture medium and a final concentration of approximately 50 nM was achieved. The transfection mixture was replaced with fresh medium after 6 hr, and the transfected cells were used for analysis at 48 hr post-transfection. I used the following siRNAs: IE1, GCGGGAGAUGUGGAUGGCUdTdT; IE2, AAACGCAUCUCCGAGUUGGACdTdT; Ago1, GAGAAGAGGUGCUCAAGAAUU; Ago2, GCACGGAAGUCCAUCUGAAUU; Ago3, GAAAUUAGCAGAUUGGUAAUU; and Ago4, GGCCAGAACUAAUAGCAAUUU. In addition, the following synthetic miR-17 duplexes were used: miR-17, pCAAAGUGCUUACAGUGCAGGUAG and miR-17*, pACUGCAGUGAAGGCACUUGUAG. The synthetic RNAs were

purchased from IDT. Antisense inhibitors of miRNAs were chemically synthesized by Dharmacon. The Synthetic miRNA inhibitors (miRIDIAN) for human miR-17 and miR-20a were used in my experiments in combination. HEK293T cells were transfected with DNA plasmids using the calcium phosphate method. HFFs were electroporated using Neon (Invitrogen) under pre-optimized conditions.

Viral mutagenesis

To generate the specific mutant virus (ToledoΔ17Seed), the UL144-145 genomic region was substituted in the Toledo-BAC using rpsL-neo cassettes. Briefly, the rpsL-neo cassettes were PCR-amplified using primers containing the sequences for the homology arms at 50 nt upstream and downstream of the target gene. The amplified DNA fragments were introduced into *Escherichia coli* DH10b cells containing the wild-type Toledo-BAC via electroporation using Gene Pulser II. The intermediate Toledo-BAC construct containing the rpsL-neo cassette was counterselected on kanamycin and streptomycin. The cassette was substituted with the mutant viral genome, containing a triple nt mutation in UL144-145. I also generated the Toledo-Revertant BAC using the

same method. The primer information is provided in Table 2.

Genome alignment between HCMV clinical strains

The genomic sequences of the following HCMV clinical strains were obtained from GenBank: Toledo (GU937742.1), VR1814 (GU179289.1), Merlin (AY446894.2), JHC (HQ380895.1), TB40/E (AY446866.1), AF1 (GU179291.1), 3301 (GQ466044.1), HAN38 (GQ396662.1), JP (GQ221975.1), U11 (GU179290.1), U8 (GU179288.1), HAN20 (GQ396663.1), 3157 (GQ221974.1), and HAN13 (GQ221973.1). Using *CLC Sequence Viewer 6* software, the DNA genome sequences of 14 clinical strains were analyzed.

Measurement of Apoptosis

Apoptotic cells were determined by flow cytometry using 7-AAD and APC-annexin V (Biolegend) according to manufacturer's instructions. Briefly, Toledo-WT or ToledoΔ17Seed-infected HFFs (4×10^5 cells) were incubated with relevant 7-AAD and APC-annexin V at room temperature for 30 min in the dark. After incubation, the stained cells were analyzed by flow cytometry using a FACS Calibur apparatus (BD Biosciences).

The 7-AAD-negative and annexin V-positive population was determined as apoptotic cells.

Statistical analysis

Unless otherwise noted, statistical significance was analyzed by the Student's t test and data represent the mean ± S.D. All data in this study were obtained at least in three independent experiments.

ACCESSION NUMBERS

The Gene Expression Omnibus (GEO) accession number for the microarray data is GSE43761.

Table 1. Primer information

Purpose	Name	F/R	Sequence	Reference
15-kb Clone recovery	Clone 1	For	AAGGAAAAAAGCGGCCGCCC GAGTCGATGCAGATGACCTG	
		Rev	CGGAATTCGTTTCACTCGCCG ATGCGGCG	
15-kb Clone recovery	Clone 2	For	AAGGAAAAAAGCGGCCGCCA GTTCACCACCGTAGCCATGG	
		Rev	CGGAATTCCACCCATTCAATC CGCATATTT T	
15-kb Clone recovery	Clone 3	For	AAGGAAAAAAGCGGCCGCAC GCCGGGAAGGGGACGACG	
		Rev	CGGAATTCCAATAATTACCCA ATATAATTT TATT	
15-kb Clone recovery	Clone 4	For	AAGGAAAAAAGCGGCCGCCC AACTAGCGACCCCAAAGGAG	
		Rev	CGGAATTCTCCCAGTAATGCG GTACTCGGT	
15-kb Clone recovery	Clone 5	For	GCTCTAGAGAACAGCACCAG CTGGCAGATT	
		Rev	CGGGATCCAGTACCAAGCGA CGATACTGAC	

15-kb Clone recovery	Clone 6	For	AAGGAAAAAAGCGGCCGCCC TGAAACCCACGTTAACCGAC	
		Rev	CGGAATTCGGGGGCGGCGGG GACTCCAC	
Overexpr ession and RT-PCR	UL144-145 RNA	For	ACGGCACGACAAATCGATGT AG	
		Rev	ATTAGGTTTCAAAATCGATAC TGT	
Reporter system	Firefly-736nt	For	GAGCGAATTCGCTTCCTGTTG TTGTTTTTAC	
		Rev	CGAACCGCGGAATTAGGTTTC AAAATCGATAC	
Reporter system	Firefly-240nt	For	GAGCGAATTCGCTTCCTGTTG TTGTTTTTAC	
		Rev	CGAACCGCGGCGAAGGCAAC AAGAAAGAGTG	
Deletion screening	Firefly-240nt Δ1	For	GAATTCGCTC TAGAATTACA CG	
		Rev	GATAATTACA GATGAGCTGT TC	
Deletion screening	Firefly-240nt Δ2	For	TGTGTGACTT CATCGTACCG TG	
		Rev	ATTCCTGCACTAAAAAAAGAA G	

Deletion screening	Firefly-240nt Δ3	For	CGTAAAGTGC TTCTTTTTTTAG	
		Rev	TGCCGACGTCAGGAAAAATA AG	
Deletion screening	Firefly-240nt Δ4	For	AAAAGTACCTAAATTCCCCA CA	
		Rev	CCCGGTGCTA TCGTGCTGTCAC	
Deletion screening	Firefly-240nt Δ5	For	CTCTTATGTAGGCGACAGCT TA	
		Rev	CCGCGGGATATCCTGCAGGC TA	
Deletion screening	Firefly-240nt Δ3-1	For	CGTAAAGTGC TTCTTTTTTTAG	
		Rev	CGTG TCTGAGTATCTG TGGG	
Deletion screening	Firefly-240nt Δ3-2	For	GTTCCGTAAAGTGCTTCTTTTT	
		Rev	TCTGAGTATCTGTGGGGAAT	
Deletion screening	Firefly-240nt Δ3-3	For	CACGGTTCCGTAAAGTGCTTC T	
		Rev	AGTATCTGTGGGGAATTTAG	
Deletion screening	Firefly-240nt Δ3-4	For	CAGACACGGTTCCGTAAAGTG C	
		Rev	TCTGTGGGGAAT TTAGGTAC	

Deletion screening	Firefly-240nt Δ3-5	For	TACTCAGACACGGTTCCGTAAA	
		Rev	TGGG GAAT TTAG GTAC TTTT	
Deletion screening	Firefly-240nt Δ3-6	For	CAGATACTCAGACACGGTTCCG	
		Rev	GAAT TTAG GTAC TTTT TGCC	
Deletion screening	Firefly-240nt Δ3-7	For	CCCACAGATACTCAGACACGGT	
		Rev	TTAG GTAC TTTT TGCC GACG	
Deletion screening	Firefly-240nt Δ3-8	For	ATTCCCCACAGATACTCAGACA	
		Rev	GTAC TTTT TGCC GACG TCAG	
Deletion screening	Firefly-240nt Δ3-9	For	CTAAATTCCCCACAGATACTCA	
		Rev	TTTT TGCC GACG TCAG GAAA	
Deletion screening	Firefly-240nt Δ3-10	For	GTACCTAAATTCCCCACAGATA	
		Rev	TGCCGACGTC AGGAAAAATAAG	
Mutagenesis	UL144-145 Seed mut	For	CCTGCACTAAAAAAAGAAGACATTTACGGAACCGTGTCTG	
		Rev	CAGACACGGTTCCGTAAATGT	

			CTTCTTTTTTTAGTGCAGG	
BAC mutagenesis	rpsL-UL144-145	For	GCTTCCTGTTGTTGTTTTTACATCACGGTACGATGAAGTCACACAGATAAGGCCTGGTGATGATGGCGGGATCG	
		Rev	CGAAGGCAACAAGAAAGAGTGACAGCACGATAGCACCGGGCTCTTATGTATCAGAAGAACTCGTCAAGAAGGCG	
BAC mutagenesis	UL144-145 amplification	For	GCTTCCTGTTGTTGTTTTTACATC	
		Rev	CGAAGGCAAC AAGAAAGAGTGAC	
HCMV genome qPCR	HCMV genome (UL150 region)	For	CCGGAATTCCGGATGCTCACACTCTATCTCTTC	
		Rev	CGCGGATCCCTACAGCTCCAAGCGCCG	
qRT-PCR	UL144-145 intergenic non-coding region	For	GCTTCCTGTTGTTGTTTTTAC	
		Rev	CGAAGGCAACAAGAAAGAGTG	
qRT-	GAPDH	For	ATCATCCCTGCCTCTACTGG	

PCR		Rev	GTCAGGTCCACCACTGACAC	
qRT-PCR	Pri-miR-17-92	For	CAGTAAAGGTAAGGAGAGCTCAATCTG	*He et al., Nature, 2005*
		Rev	CATACAACCACTAAGCTAAAGAATAATCTGA	
qRT-PCR	Pri-miR-125b-1	For	CCATACCACCTGTTTGTTGCATCT	*Zhou et al., Nucleic Acids Res., 2010*
		Rev	CTGAGAGGAGCGCAACAATGT	
qRT-PCR	Pri-miR-29a	For	CCAACCCTCACGACCTTCTG	*Zhou et al., Nucleic Acids Res., 2010*
		Rev	TCCTCTCAGCAGTCAGCATCA	
qRT-PCR	Pri-miR-199a-1	For	GGTTCTGCAGGATGGATAGC	
		Rev	GGGTGGTGGAAAATGACACT	

VI. REFERENCES

Altuvia, Y., Landgraf, P., Lithwick, G., Elefant, N., Pfeffer, S., Aravin, A., Brownstein, M.J., Tuschl, T., and Margalit, H. (2005). Clustering and conservation patterns of human microRNAs. Nucleic Acids Res *33*, 2697-2706.

Bernstein, E., Caudy, A.A., Hammond, S.M., and Hannon, G.J. (2001). Role for a bidentate ribonuclease in the initiation step of RNA interference. Nature *409*, 363-366.

Britt, W. (2008). Manifestations of human cytomegalovirus infection: proposed mechanisms of acute and chronic disease. Curr Top Microbiol Immunol *325*, 417-470.

Cazalla, D., Yario, T., and Steitz, J.A. (2010). Down-regulation of a host microRNA by a Herpesvirus saimiri noncoding RNA. Science *328*, 1563-1566.

Chang, T.C., and Mendell, J.T. (2007). microRNAs in vertebrate physiology and human disease. Annu Rev Genomics Hum Genet *8*, 215-239.

Das, R., and Baker, D. (2007). Automated de novo prediction of native-like RNA tertiary structures. Proc Natl Acad Sci U S A *104*, 14664-14669.

Goodrum, F., Reeves, M., Sinclair, J., High, K., and Shenk, T. (2007). Human cytomegalovirus sequences expressed in latently infected individuals promote a latent infection in vitro. Blood *110*, 937-945.

Hagemeier, C., Caswell, R., Hayhurst, G., Sinclair, J., and Kouzarides, T. (1994). Functional interaction between the HCMV IE2 transactivator and the retinoblastoma protein. EMBO J *13*, 2897-2903.

Hahn, G., Revello, M.G., Patrone, M., Percivalle, E., Campanini, G., Sarasini, A., Wagner, M., Gallina, A., Milanesi, G., Koszinowski, U., *et al.* (2004). Human cytomegalovirus UL131-128 genes are indispensable for virus growth in endothelial cells and virus transfer to leukocytes. J Virol *78*, 10023-10033.

He, L., Thomson, J.M., Hemann, M.T., Hernando-Monge, E., Mu, D., Goodson, S., Powers, S., Cordon-Cardo, C., Lowe, S.W., Hannon, G.J., *et al.* (2005). A microRNA polycistron as a potential human oncogene. Nature *435*, 828-833.

He, R., Ma, Y., Qi, Y., Wang, N., Li, M., Ji, Y., Sun, Z., Jiang, S., and Ruan, Q. (2011). Characterization of the transcripts of human cytomegalovirus UL144. Virol J *8*, 299.

Hutvagner, G., McLachlan, J., Pasquinelli, A.E., Balint, E., Tuschl, T., and Zamore, P.D. (2001). A cellular function for the RNA-interference enzyme Dicer in the maturation of the let-7 small temporal RNA. Science *293*, 834-838.

Ketting, R.F., Fischer, S.E., Bernstein, E., Sijen, T., Hannon, G.J., and Plasterk, R.H. (2001). Dicer functions in RNA interference and in synthesis of small RNA involved in developmental timing in C. elegans. Genes Dev *15*, 2654-2659.

Khvorova, A., Reynolds, A., and Jayasena, S.D. (2003). Functional siRNAs and miRNAs exhibit strand bias. Cell *115*, 209-216.

Kim, Y., Lee, S., Kim, S., Kim, D., Ahn, J.H., and Ahn, K. (2012). Human cytomegalovirus clinical strain-specific microRNA miR-UL148D targets the human chemokine RANTES during infection. PLoS Pathog *8*, e1002577.

Knight, S.W., and Bass, B.L. (2001). A role for the RNase III enzyme DCR-1 in RNA interference and germ line development in Caenorhabditis elegans. Science *293*, 2269-2271.

Krol, J., Loedige, I., and Filipowicz, W. (2010). The widespread regulation of microRNA biogenesis, function and decay. Nat Rev Genet *11*, 597-610.

Lee, Y., Ahn, C., Han, J., Choi, H., Kim, J., Yim, J., Lee, J., Provost, P., Radmark, O., Kim, S.*, et al.* (2003). The nuclear RNase III Drosha initiates microRNA processing. Nature *425*, 415-419.

Lee, Y., Kim, M., Han, J., Yeom, K.H., Lee, S., Baek, S.H., and Kim, V.N. (2004). MicroRNA genes are transcribed by RNA polymerase II. EMBO J *23*, 4051-4060.

Libri, V., Helwak, A., Miesen, P., Santhakumar, D., Borger, J.G., Kudla, G., Grey, F., Tollervey, D., and Buck, A.H. (2011). Murine cytomegalovirus encodes a miR-27 inhibitor disguised as a target. Proc Natl Acad Sci U S A *109*, 279-284.

Luxan, G., Casanova, J.C., Martinez-Poveda, B., Prados, B., D'Amato, G., Macgrogan, D., Gonzalez-Rajal, A., Dobarro, D., Torroja, C., Martinez, F.*, et al.* Mutations in the NOTCH pathway regulator MIB1 cause left ventricular noncompaction cardiomyopathy. Nat Med *19*, 193-201.

Ma, Y., Wang, N., Li, M., Gao, S., Wang, L., Zheng, B., Qi, Y., and Ruan, Q. (2012). Human CMV transcripts: an overview. Future Microbiol *7*, 577-593.

Marcinowski, L., Tanguy, M., Krmpotic, A., Radle, B., Lisnic, V.J., Tuddenham,

L., Chane-Woon-Ming, B., Ruzsics, Z., Erhard, F., Benkartek, C.*, et al.* (2012). Degradation of cellular mir-27 by a novel, highly abundant viral transcript is important for efficient virus replication in vivo. PLoS Pathog *8*, e1002510.

Margolis, M.J., Pajovic, S., Wong, E.L., Wade, M., Jupp, R., Nelson, J.A., and Azizkhan, J.C. (1995). Interaction of the 72-kilodalton human cytomegalovirus IE1 gene product with E2F1 coincides with E2F-dependent activation of dihydrofolate reductase transcription. J Virol *69*, 7759-7767.

Mavrakis, K.J., Wolfe, A.L., Oricchio, E., Palomero, T., de Keersmaecker, K., McJunkin, K., Zuber, J., James, T., Khan, A.A., Leslie, C.S.*, et al.* (2010). Genome-wide RNA-mediated interference screen identifies miR-19 targets in Notch-induced T-cell acute lymphoblastic leukaemia. Nat Cell Biol *12*, 372-379.

McCormick, A.L. (2008). Control of apoptosis by human cytomegalovirus. Curr Top Microbiol Immunol *325*, 281-295.

Mendell, J.T. (2008). miRiad roles for the miR-17-92 cluster in development and disease. Cell *133*, 217-222.

Mu, P., Han, Y.C., Betel, D., Yao, E., Squatrito, M., Ogrodowski, P., de Stanchina, E., D'Andrea, A., Sander, C., and Ventura, A. (2009). Genetic dissection of the miR-17~92 cluster of microRNAs in Myc-induced B-cell lymphomas. Genes Dev *23*, 2806-2811.

Murphy, E., Yu, D., Grimwood, J., Schmutz, J., Dickson, M., Jarvis, M.A., Hahn, G., Nelson, J.A., Myers, R.M., and Shenk, T.E. (2003). Coding potential of laboratory and clinical strains of human cytomegalovirus. Proc Natl Acad Sci

U S A *100*, 14976-14981.

Nowak, M.A., and May, R.M. (2000). Virus dynamics : mathematical principles of immunology and virology (Oxford: Oxford University Press).

Olive, V., Bennett, M.J., Walker, J.C., Ma, C., Jiang, I., Cordon-Cardo, C., Li, Q.J., Lowe, S.W., Hannon, G.J., and He, L. (2009). miR-19 is a key oncogenic component of mir-17-92. Genes Dev *23*, 2839-2849.

Olive, V., Jiang, I., and He, L. (2010). mir-17-92, a cluster of miRNAs in the midst of the cancer network. Int J Biochem Cell Biol *42*, 1348-1354.

Pall, G.S., and Hamilton, A.J. (2008). Improved northern blot method for enhanced detection of small RNA. Nat Protoc *3*, 1077-1084.

Penfold, M.E., Dairaghi, D.J., Duke, G.M., Saederup, N., Mocarski, E.S., Kemble, G.W., and Schall, T.J. (1999). Cytomegalovirus encodes a potent alpha chemokine. Proc Natl Acad Sci U S A *96*, 9839-9844.

Poole, E., King, C.A., Sinclair, J.H., and Alcami, A. (2006). The UL144 gene product of human cytomegalovirus activates NFkappaB via a TRAF6-dependent mechanism. EMBO J *25*, 4390-4399.

Revello, M.G., and Gerna, G. (2010). Human cytomegalovirus tropism for endothelial/epithelial cells: scientific background and clinical implications. Rev Med Virol *20*, 136-155.

Santhakumar, D., Forster, T., Laqtom, N.N., Fragkoudis, R., Dickinson, P., Abreu-Goodger, C., Manakov, S.A., Choudhury, N.R., Griffiths, S.J., Vermeulen, A.*, et al.* (2010). Combined agonist-antagonist genome-wide functional

screening identifies broadly active antiviral microRNAs. Proc Natl Acad Sci U S A *107*, 13830-13835.

Schwarz, D.S., Hutvagner, G., Du, T., Xu, Z., Aronin, N., and Zamore, P.D. (2003). Asymmetry in the assembly of the RNAi enzyme complex. Cell *115*, 199-208.

Shan, S.W., Lee, D.Y., Deng, Z., Shatseva, T., Jeyapalan, Z., Du, W.W., Zhang, Y., Xuan, J.W., Yee, S.P., Siragam, V.*, et al.* (2009). MicroRNA MiR-17 retards tissue growth and represses fibronectin expression. Nat Cell Biol *11*, 1031-1038.

Sinclair, J., and Sissons, P. (2006). Latency and reactivation of human cytomegalovirus. J Gen Virol *87*, 1763-1779.

Sinzger, C., Digel, M., and Jahn, G. (2008). Cytomegalovirus cell tropism. Curr Top Microbiol Immunol *325*, 63-83.

Song, Y.J., and Stinski, M.F. (2002). Effect of the human cytomegalovirus IE86 protein on expression of E2F-responsive genes: a DNA microarray analysis. Proc Natl Acad Sci U S A *99*, 2836-2841.

Stern-Ginossar, N., Weisburd, B., Michalski, A., Le, V.T., Hein, M.Y., Huang, S.X., Ma, M., Shen, B., Qian, S.B., Hengel, H.*, et al.* (2012). Decoding human cytomegalovirus. Science *338*, 1088-1093.

Sylvestre, Y., De Guire, V., Querido, E., Mukhopadhyay, U.K., Bourdeau, V., Major, F., Ferbeyre, G., and Chartrand, P. (2007). An E2F/miR-20a autoregulatory feedback loop. J Biol Chem *282*, 2135-2143.

Teng, M.W., Bolovan-Fritts, C., Dar, R.D., Womack, A., Simpson, M.L., Shenk,

T., and Weinberger, L.S. (2012). An endogenous accelerator for viral gene expression confers a fitness advantage. Cell *151*, 1569-1580.

Wang, F.Z., Weber, F., Croce, C., Liu, C.G., Liao, X., and Pellett, P.E. (2008). Human cytomegalovirus infection alters the expression of cellular microRNA species that affect its replication. J Virol *82*, 9065-9074.

Wang, N., Ma, Y., Sun, Z., Qi, Y., Ji, Y., He, R., Li, M., and Ruan, Q. (2011). Transcriptional features and transcript structure of UL145 in different strains of human cytomegalovirus. J Med Virol *83*, 2151-2156.

Wang, W., Taylor, S.L., Leisenfelder, S.A., Morton, R., Moffat, J.F., Smirnov, S., and Zhu, H. (2005). Human cytomegalovirus genes in the 15-kilobase region are required for viral replication in implanted human tissues in SCID mice. J Virol *79*, 2115-2123.

Wills, M.R., Ashiru, O., Reeves, M.B., Okecha, G., Trowsdale, J., Tomasec, P., Wilkinson, G.W., Sinclair, J., and Sissons, J.G. (2005). Human cytomegalovirus encodes an MHC class I-like molecule (UL142) that functions to inhibit NK cell lysis. J Immunol *175*, 7457-7465.

Zhang, G., Raghavan, B., Kotur, M., Cheatham, J., Sedmak, D., Cook, C., Waldman, J., and Trgovcich, J. (2007). Antisense transcription in the human cytomegalovirus transcriptome. J Virol *81*, 11267-11281.

Zhu, H., Shen, Y., and Shenk, T. (1995). Human cytomegalovirus IE1 and IE2 proteins block apoptosis. J Virol *69*, 7960-7970.

VII. 국문 초록

인간 거대세포바이러스(HCMV)의 임상형 균주의 높은 독성은 UL/b' 유전체 부분의 15 kb 와 깊은 관련이 있는 것으로 간주되고 있다. 본 연구에서는 유전자간 RNA 서열인 마이크로 RNA 분해요소(microRNA Decay Element: miRDE)가 선택적으로 두 마이크로 RNA, miR-17 과 miR-20a 를 분해하는 것을 관찰하였다. 이 miRDE 는 바이러스 균주 간에 높은 보존력을 보였다. 일반적인 miRNA-mRNA 관계와는 다르게, miRNA-miRDE 관계는 miRDE 의 발현을 억제하지 않는 것으로 관찰되었다. miRDE 의 miRNA 결합 부위를 다른 miRNA 에 대한 서열로 교체하였을 때 특이성도 함께 교체되는 것을 밝혔다. 또한 HCMV 의 용균성 감염 시에 miRDE 에 의한 miRNA 분해는 바이러스의 용균성 복제를 가속화시키는 것으로 보였다. 이렇게 바이러스가 숙주 세포의 miRNA 를 조절하는 것은 임상형 바이러스의 이해에 대한 새로운 국면을 제시하는 것이라고 할 수 있다.

주요어: 인간 거대세포바이러스, 마이크로 RNA, 임상형 바이러스, 마이크로 RNA 분해요소.

학번: 2008-22751

VIII. APPENDIX

EDUCATION

2008-2014 present **Ph.D**., Biology, Seoul National University
2004-2008 **B.S.**, Biology, Seoul National University

PUBLICATIONS

Sanghyun Lee, Jaewon Song, Sungchul Kim, Jongkyu Kim, Yujin Hong, Youngkyun Kim, Donghyun Kim, Daehyun Baek and Kwangseog Ahn, (2013) Selective Degradation of host MicroRNAs by an Intergenic HCMV Non-Coding RNA Accelerates Virus Production,
Cell Host & Microbe, 13(6), 678-690.

Youngkyun Kim*, **Sanghyun Lee***, Sungchul Kim, Donghyun Kim, Jin-Hyun Ahn and Kwangseog Ahn, (2012) Human Cytomegalovirus Clinical Strain-Specific microRNA miR-UL148D Targets the Human Chemokine RANTES during Infection, *PLoS Pathog*, 8(3), 1-12.
(***** *Co-first author*)

Sungchul Kim, **Sanghyun Lee**, Jinwook Shin, Youngkyun Kim, Irini Evnouchidou, Donghyun Kim, Young-Kook Kim, Young-Eui Kim, Jin-Hyun Ahn, Stanley R Riddell, Efstratios Stratikos, V Narry Kim and Kwangseog Ahn. (2011) Human cytomegalovirus microRNA miR-US4-1 inhibits CD8+ T cell responses by targeting the aminopeptidase ERAP1, *Nat. Immunol*. 12(10):984-91.